COMPARING TROPOPAUSE-PENETRATING CONVECTION IDENTIFICATIONS DERIVED FROM NEXRAD AND GOES OVER THE CONTIGUOUS UNITED STATES

A Dissertation

by

JOHN WILLIAM COONEY

Submitted to the Office of Graduate and Professional Studies of
Texas A&M University
in partial fulfillment of the requirements for the degree of

DOCTOR OF PHILOSOPHY

Chair of Committee,	Kenneth Bowman
Committee Members,	Anita Rapp
	Christopher Nowotarski
	Andrew Klein
Head of Department,	Ramalingam Saravanan

May 2020

Major Subject: Atmospheric Sciences

ABSTRACT

In this paper overshooting top (OT) refers to a convective updraft that extends above the primary lapse-rate tropopause. OTs are a result of powerful updrafts that rapidly transport air from the lower troposphere to the lower stratosphere. They can initiate gravity waves and mixing of air across the tropopause. Within the last decade remote-sensing observations from satellites and radars have been used to estimate the altitudes of OTs, but the results have not been consistent. To understand the reasons for the differences and to improve the accuracy of tropopause-overshooting top identifications, this study compares overshooting convection identified using NEXRAD radar reflectivity data with two approaches that use GOES IR data. The study region covers a large part of the contiguous United States during selected active convection dates in 2004 and 2006. NEXRAD can estimate the altitude of echo tops directly from the radar pointing geometry. The GOES methods use IR brightness temperature as a proxy to estimate the cloud top relative to the tropopause and surrounding cloud. GOES IR Version 1 retrievals of OTs are heavily weighted towards horizontal temperature gradients within the cloud, while GOES IR Version 2 gives more weight to temperature differences between the potential top and tropopause. We found Version 1 overestimates the frequency of OTs, particularly in the southeast US. The frequency is overestimated because too much weight is given to horizontal temperature gradients within the cloud and not enough weight is given to the temperature difference between the cloud top and tropopause. GOES IR Version 1 erroneously tags events that are warmer than the tropopause and located outside of strong updraft regions as overshoots. Version 2 agrees much better with NEXRAD OT retrievals, particularly when the spatial matching conditions are slightly relaxed.

ACKNOWLEDGEMENTS

Funding for this work was provided by the National Science Foundation through grants AGS-1522906 and AGS-1522910 to Texas A&M University and the University of Oklahoma, respectively. Radar data were downloaded from the NOAA National Centers for Environmental Information (http://www.ncdc.noaa.gov). The NEXRAD data files were translated to netCDF format using the NOAA Weather and Climate Toolkit (https://www.ncdc.noaa.gov/wct/). ECMWF ERA-Interim reanalysis data were downloaded from the National Center for Atmospheric Research Research Data Archive (NCAR RDA; http://rda.ucar.edu/datasets/ds627.0/). GridRad data are available at the NCAR RDA (http://rda.ucar.edu/datasets/ds841.0/). GOES OT, raw MERRA-1 and MERRA-2 data, and MERRA-1 and MERRA-2 tropopauses were provided by Mr. Kristopher Bedka and his team at the NASA Langley Research Center.

CONTRIBUTORS AND FUNDING SOURCES

Contributors

This work was supported by a dissertation committee consisting of Dr. Kenneth Bowman (advisor), Dr. Anita Rapp, and Dr. Christopher Nowotarski of the Department of Atmospheric Sciences and Dr. Andrew Klein of the Department of Geography. NEXRAD radar data were downloaded from the NOAA National Centers for Environmental Information (http://www.ncdc.noaa.gov). This initiative is supported by National Center for Atmospheric Research (NCAR) under the sponsorship of the National Science Foundation (NSF). The NEXRAD data files were translated to netCDF format using the NOAA Weather and Climate Toolkit (https://www.ncdc.noaa.gov/wct/). ECMWF ERA-Interim reanalysis data were downloaded from the National Center for Atmospheric Research Research Data Archive (NCAR RDA; http://rda.ucar.edu/datasets/ds627.0/). Mr. Kristopher Bedka and his team at the National Aeronautics and Space Administration (NASA) Langley Research Center (LRC) produced the two versions of the Geostationary Operational Environmental Satellites (GOES) overshoot detection data for us to use. MERRA and MERRA-2 data were also provided by Mr. Kristopher Bedka and his team at the NASA LRC. Dr. Cameron Homeyer at the University of Oklahoma provided his expertise in answering questions regarding tropopause-overshooting convective events.

Funding Sources

Funding for this work was provided by the National Science Foundation through grants AGS-1522906 and AGS-1522910 to Texas A&M University and the University of Oklahoma, respectively.

NOMENCLATURE

CONUS	Contiguous US
ERA-I	ERA-Interim
FAA	Federal Aviation Administration
GOES	Geostationary Operational Environmental Satellites
IR	Infrared
MCC	Mesoscale Convective Complex
MERRA	Modern-Era Retrospective Analysis for Research and Applications
MERRA-2	Modern-Era Retrospective Analysis for Research and Applications Version 2
NASA	National Aeronautics and Space Administration
NCEI	National Center for Environmental Information
NEXRAD	Next Generation Weather Radar Network
NOAA	National Oceanic and Atmospheric Administration
OT	Overshooting Top
UTLS	Upper Troposphere and Lower Stratosphere
WMO	World Meteorological Organization

TABLE OF CONTENTS

Page

LIST OF FIGURES

FIGURE Page

LIST OF TABLES

TABLE Page

1. INTRODUCTION AND BACKGROUND

The Glossary of Meteorology (AMS, 2019) defines an overshooting top (OT) as a "domelike protrusion above a cumulonimbus anvil, representing the intrusion of an updraft through its equilibrium level". In this paper we focus on overshooting tops that extend above the primary lapse-rate tropopause into the lower stratosphere.

Deep convective events contain thermally driven, turbulent updrafts capable of rapidly lifting lower tropospheric and boundary layer air to the Upper Troposphere and Lower Stratosphere (UTLS) (*Solomon et al.*, 2016; *Cooney et al.*, 2018). Strong updrafts that are capable of overshooting the tropopause are common within deep convective storms over the contiguous US (CONUS), with tens of thousands of OTs occurring in a given year (*Cooney et al.*, 2018). OTs are known to be closely connected to the seasonal evolution of convection and the tropopause. Overshoots occur more frequently during the early summer months, when the tropopause altitude is lower, than later in the summer, when the tropopause altitude is higher (*Cooney et al.*, 2018). The tropopause height likely influences the geographic distribution of overshoots as well. In the US, for example, convection is very active in the southeast and plains regions, but the tropopause in the southeast is typically higher, reducing the frequency of overshooting there.

The boundaries of updrafts, including the OT, are turbulent, which leads to irreversible mixing of air between the stratosphere and troposphere, altering the composition of both the upper troposphere and lower stratosphere. Aircraft observations of OTs show the downward transport of ozone-rich stratospheric air into the upper troposphere (*Pan et al.*, 2014). Within a storm system containing updrafts that surpassed the local tropopause by as much as 3 km, *Pan et al.* (2014) measured the upper troposphere mixing ratio of ozone 50-140 ppbv higher than in areas external to the storm system. In addition to downward transport, OTs inject water into the lower stratosphere, predominantly in the form of ice, where it can sublimate and moisten the dry stratosphere. In a case-study of a mesoscale convective complex (MCC) in Minnesota and Wisconsin consisting of several overshooting tops, *Smith et al.* (2017) uses aircraft measurements and a back trajectory

analysis to assess the impact on the UTLS composition. The authors estimate that approximately 6.6-13.5 kt of water were irreversibly injected into the stratosphere by the MCC, which corresponds to ∼0.0007-0.0013% of the stratospheric water vapor reservoir (*Smith et al.*, 2017). *Herman et al.* (2017) analyzes JPL Laser Hygrometer (JLH Mark2) observations of stratospheric water vapor mixing ratios. The results show a 4 to 6 ppmv enhancement above the typical < 5 ppmv background of the stratospheric overworld (above the ∼380 K isentrope level) in the 1 to 7 days after an OT event. Although these numbers are small and localized, changes in the stratospheric composition of this magnitude can have a significant impact on chemistry and Earth's radiation balance (*Holton et al.*, 1995; *Forster and Shine*, 1999a; *Stohl et al.*, 2003; *Dessler and Sherwood*, 2004; *Anderson et al.*, 2012, 2017). For example, *Forster and Shine* (1999b) estimates that, between 1979 and 1997, increases in stratospheric water vapor increased the surface equilibrium temperature 0.11 K, ∼44% of the increase from atmospheric carbon dioxide during that period (0.25 K). This increase in stratospheric water vapor is not primarily due to OTs, but the estimate illustrates how stratospheric water vapor changes can impact the surface equilibrium temperature.

In addition to upper troposphere and lower stratosphere composition changes, OTs produce turbulence through the generation of gravity waves, which can be dangerous for aviation (*Heymsfield et al.*, 1991; *Lane et al.*, 2003; *Bedka et al.*, 2010). Using a two-dimensional calculation of a tropopause-overshooting updraft, *Lane et al.* (2003) estimates turbulence can be generated up to 3 km above the cloud top and 30 km in the horizontal. The Federal Aviation Administration (FAA) estimates that over 300 people have been injured by turbulence between 2009 and 2017 (*FAA*, 2019). Therefore, it is important to accurately identify tropopause-overshooting events.

Within the last decade, remote-sensing observations from satellites, radars, and lidars have been used to estimate cloud tops relative to the tropopause. Some methods are essentially geometric (radar, lidar, stereo), while others are indirect (infrared temperature or visible texture). Two cloud detecting satellites, CloudSat and CALIPSO, are sun-synchronous, nadir-pointing, low Earth-orbiting satellites that are part of the National Aeronautics and Space Administration (NASA) "Afternoon" constellation of satellites (A-Train). The Cloud-Aerosol Lidar with Orthogonal Po-

larization (CALIOP), aboard the CALIPSO satellite, and the Cloud Profiling Radar (CPR), aboard CloudSat have high spatial resolution [335-1000 m $\times$ 30-60 m and 1.1 km $\times$ 240 m (horizontal $\times$ vertical), respectively] and are very sensitive to cloud particles, which makes them ideal for identifying cloud tops. However, the narrow viewing swaths of the instruments require the satellite to pass directly above an overshooting event. Also, A-Train satellite overpasses do not coincide with the diurnal peak in deep convective activity over the continents, so many OTs are not observed (*Homeyer et al.*, 2014).

To provide better spatial and temporal coverage, *Cooney et al.* (2018) identifies OTs using data from the dense Next Generation Weather Radar network (NEXRAD) over the CONUS using methods developed in *Homeyer and Kumjian* (2015) and *Solomon et al.* (2016). In a 10-year climatology of March-August overshoots, *Cooney et al.* (2018) uses horizontally-polarized radar reflectivity Z_H on a $\sim$2 km $\times$ 1 km (horizontal $\times$ vertical) grid and a 10 dBZ reflectivity threshold to estimate echo-top altitude z_e. OTs are identified by comparing NEXRAD z_e with the primary lapse-rate tropopause altitude, defined by the World Meteorological Organization (WMO) as the lowest level at which the lapse-rate decreases to 2 K/km or less, provided also the average lapse-rate between this level and all higher levels within 2 km does not exceed 2 K/km (*WMO*, 1957).

NEXRAD radars, however, have a limited sensitivity to small particles, so the echo-top altitude is generally below the cloud top altitude, which may miss some tropopause-overshooting events. Lower reflectivity thresholds would provide a better estimate of the cloud top but could also result in a higher frequency of errors and artifacts (*Cooney et al.*, 2018). *Cooney et al.* (2018) uses 10 dBZ because it provides a good balance between sensitivity and noise. A comparison of 10 dBZ echo-top altitudes from NEXRAD and CloudSat CPR shows that NEXRAD z_e are consistent with the satellite observations (*Cooney et al.*, 2018). The two estimates are essentially unbiased with respect to each other, with differences ranging from 0.5 to 1 km. Because NEXRAD radar coverage across the US is not uniform, larger differences between NEXRAD and CloudSat typically occur in areas of sparse radar coverage (*Cooney et al.*, 2018). The vertical resolution near the tropopause is inadequate in regions with sparse radar coverage, which may result in missed OT detections.

The imager aboard the Geostationary Operational Environmental Satellites (GOES) is also capable of detecting overshooting tops with good spatial and temporal resolution. In order to provide turbulence warnings for aircraft, *Bedka and Khlopenkov* (2016) uses OT detection criteria described in *Bedka et al.* (2010) to create an overshoot pattern recognition algorithm. The algorithm attempts to quantify how much a cluster of pixels resemble an OT on the basis of spatial variations in GOES infrared channel images. Deep convection typically has a spatially coherent area of cold brightness temperature (T_b) with a distinct anvil edge, marking the transition from cloud to the warmer Earth surface (*Bedka and Khlopenkov*, 2016). Anomalously cold T_b in the image are caused by persistent moist-adiabatic ascent, allowing updrafts to be much colder than the temperature in the surrounding environment (*Bedka and Khlopenkov*, 2016). By using the IR imager channel to obtain surface and cloud top temperatures (*Hillger et al.*, 2003), OTs within an anvil appear as small clusters of cold pixels relative to surrounding anvil (*Bedka et al.*, 2010). IR T_b colder than the tropopause temperature likely represent an intrusion into the lower stratosphere.

Using temperature differences to identify overshooting, however, is a difficult task. Parcels within updrafts rise and cool pseudo-adiabatically, relative to the environment, so it is possible for remotely-sensed temperatures of cloud tops to be colder than the tropopause but not actually overshoot it. Geostationary satellites also observe above anvil cirrus plumes form in the lower stratosphere (*Fujita*, 1981; *Negri*, 1982; *Adler and Mack*, 1986; *Heymsfield et al.*, 1991; *Levizzani and Setvak*, 1996). These cirrus clouds can be blown downstream from OT events and may be incorrectly flagged as distinct OTs. In addition to false OT detections, using temperature differences as a proxy can miss OTs. Satellite observations and numerical-model simulations have suggested that some long-lived OTs can actually be warmer than the surrounding anvil and tropopause, in part due to turbulent mixing between the OT and the warmer stratosphere (*Adler and Mack*, 1986; *Setvak et al.*, 2010; *Bedka and Khlopenkov*, 2016). This is most often prevalent in environments with a sharp temperature inversion just above the tropopause. *Setvak et al.* (2010) noted that IR-based tropopause-overshoot detection methods likely cannot observe these long-lived and anomalously warm OTs. In order to address the uncertainty in identifying potential OT candidates from GOES

IR data, *Bedka and Khlopenkov* (2016) assigns an OT probability based on a logistic regression of metrics that were determined to be useful for identifying overshooting events in *Bedka et al.* (2010). Depending on the magnitude of overshooting and the quality control settings applied, the IR method has a false-alarm rate that ranges from 4% to 39% and a probability of OT detection rate that ranges from 46% to 81% (*Bedka and Khlopenkov*, 2016).

The methods described in *Cooney et al.* (2018) and *Bedka and Khlopenkov* (2016) are both able to detect tropopause-overshooting updrafts over the contiguous United States with high temporal and spatial resolution, but the results are not entirely consistent. Figure 1.1 shows that the GOES and NEXRAD methods find very different geographic distributions of OTs. *Bedka et al.* (2010) finds a majority of OTs in the southeast United States (Figure 1.1a), while *Cooney et al.* (2018) finds the maximum occurrence in the central plains, with very few OTs in the southeast (Figure 1.1b). In order to improve the reliability of overshooting top identifications of both methods, the goal of this study is to analyze the differences between the two tropopause-overshoot detection schemes. This study compares the NEXRAD and GOES approaches over the eastern two-thirds of the United States for selected dates with high convective activity in 2004 and 2006. Two versions of the GOES OT detection method are tested against the *Cooney et al.* (2018) NEXRAD analysis. The first version uses the methods described in *Bedka and Khlopenkov* (2016), while the second version includes a number of revisions (discussed in Section 2.4) to the algorithm.

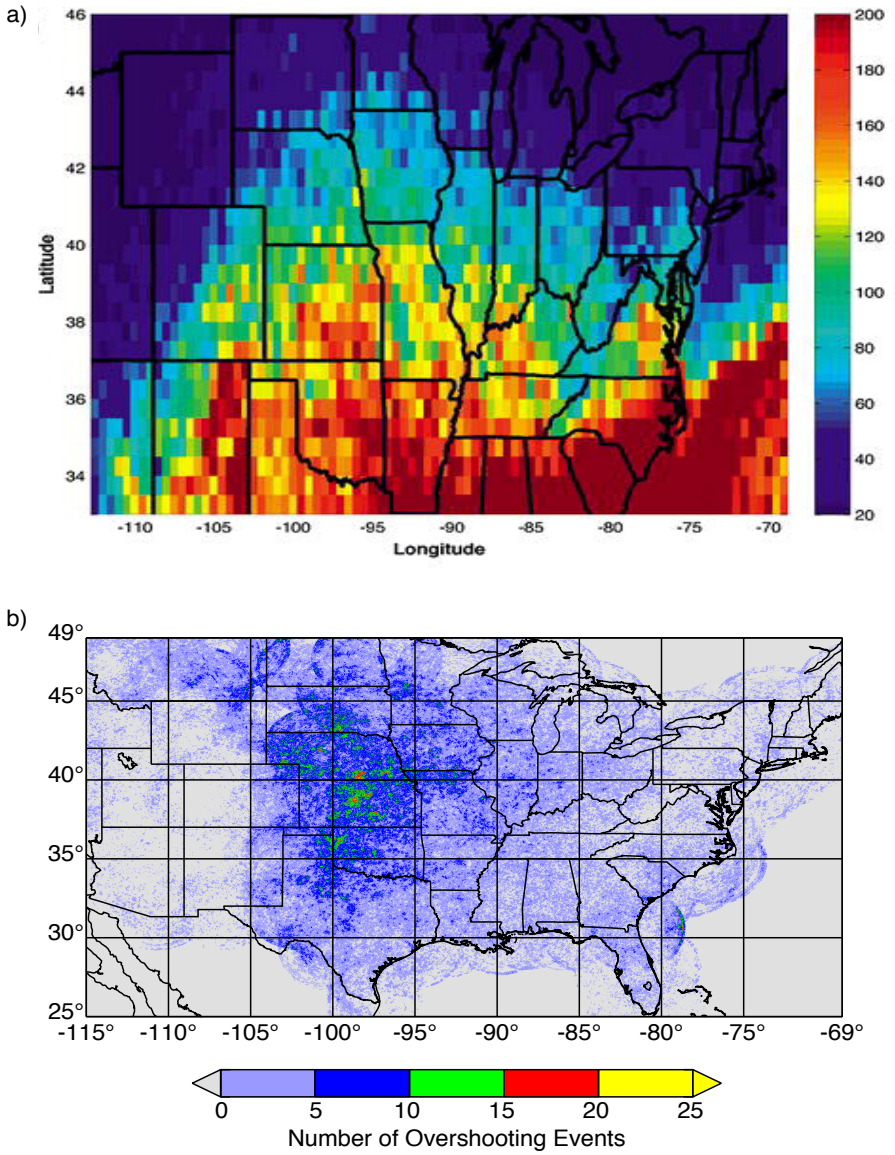

Figure 1.1: (a) A climatology of OTs detected by the IR-texture method using GOES-12 imagery from April to September 2004-2008. Reprinted from (*Bedka et al.*, 2010). (b) A climatology of OTs reaching at least 1 km above the tropopause using the NEXRAD radar analysis from March to August 2004-2013. Reprinted from (*Cooney et al.*, 2018).

2. DATA

2.1 Meteorological Analyses

Reanalyses combine models with observations in space and time into a spatially complete meteorological dataset (*Rienecker et al.*, 2011). Subtle differences distinguish reanalyses from each other; they may use different input data and may contain different physical parameterizations which leads to different estimates of the atmospheric state (*Peng*, 2014). The NEXRAD OT analysis uses 6-hourly meteorological data from the European Centre for Medium-Range Weather Forecasts (EMCWF) Interim Reanalysis (ERA-I) (*Dee et al.*, 2011). The primary lapse-rate tropopause height (Z_{ERA}) and temperature (T_{ERA}) are computed on the ERA-I grid [$\sim$0.7° $\times$ $\sim$0.7°] from the ERA-I geopotential height, pressure, and temperature profiles using the WMO definition of the lapse-rate tropopause (*WMO*, 1957). Z_{ERA} and T_{ERA} are linearly interpolated onto the hourly NEXRAD data grid for analysis. The 250 hPa eastward (u) and northward (v) wind components are used in this study to show wind speed and direction in the UTLS.

The GOES OT algorithms use meteorological data from the 6-hourly NASA Modern-Era Retrospective analysis for Research and Applications Version 1 (MERRA) and Version 2 (MERRA-2). MERRA-2 data was not operational when GOES OT Version 1 was created. MERRA-2 uses an upgraded version of the Goddard Earth Observing System (GEOS) model data assimilation system and the Global Statistical Interpolation (GSI) analysis scheme (*Bosilovich and Lucchesi*, 2016). MERRA data [$\sim$0.66° $\times$ $\sim$0.5°] and MERRA-2 data [$\sim$0.625° $\times$ $\sim$0.5°] are interpolated onto the GOES IR data longitude-latitude grid for analysis (*Rienecker et al.*, 2011; *Bosilovich and Lucchesi*, 2016). MERRA and MERRA-2 datasets are also on an irregular vertical grid extending from Earth's surface to 0.01 hPa.

Parameters from the MERRA reanalysis include the convective available potential energy (CAPE), most-unstable equilibrium temperature, and wind shear values which are used in *Bedka and Khlopenkov* (2016) to suppress false OT detections. The tropopause temperature (T_{MERRA}) is derived from

MERRA reanalysis geopotential height, pressure, and temperature. The GOES Version 2 algorithm uses MERRA-2 rather than MERRA data, as MERRA-2 should provide a better estimate of the tropopause. Parameters from the MERRA-2 reanalysis include geopotential height, pressure, and temperature, which are used in the Version 2 scheme to derive tropopause temperature (T_{MERRA2}), tropopause height (Z_{MERRA2}), and tropopause pressure (p_{MERRA2}). The Version 2 GOES OT detection scheme smooths T_{MERRA2} along gradients that favor temperatures on the cold side in order to avoid 'boxy artifacts' in the end product.

2.2 NEXRAD OT Analysis

The NEXRAD OT detection algorithm uses hourly GridRad analyses, which are based on WSR-88D radar data obtained from the National Oceanic and Atmospheric Administration (NOAA) National Center for Environmental Information (NCEI) (*Homeyer and Kumjian*, 2015; *Solomon et al.*, 2016; *Homeyer and Bowman*, 2017; *Cooney et al.*, 2018). GridRad data are stored on a regular longitude-latitude-altitude grid with a resolution of $0.02° \times 0.02° \times 1$ km [~ 2 km $\times 2$ km $\times 1$ km]. The analysis domain is the rectangular region from 115°W to 69°W and 25°N to 49°N (shown in Figure 4.1), which covers most of the continental United States. Each analysis uses all available radar azimuth scans (elevation angles) within a $\pm$3.8-minute time window centered on hourly analysis times. Observations from multiple radars are merged using weights that depend on the distance from the radar to the analysis location and on the time difference from the nominal analysis time (*Homeyer and Bowman*, 2017). The data include weighted-average radar reflectivity (Z_H) from multiple observations, averaging weights, number of azimuth scans observing each volume, and the number of azimuth scans with echo in each volume.

Tropopause-penetrating convection is identified by comparing the radar echo-top height (z_e) to the primary lapse-rate tropopause height derived from the ERA-I reanalysis (Z_{ERA}). A NEXRAD OT is defined as a contiguous group of overshooting GridRad columns. Due to uncertainties in z_e and Z_{ERA}, *Cooney et al.* (2018) requires overshoots to have echo tops with $z_r \geq 1$ km, where $z_r = z_e - Z_{ERA}$. To allow for a consistent comparison with the GOES overshoot algorithm, a

NEXRAD overshoot is defined in this paper as a contiguous region with $z_r > 0$ km, denoted here as an OTN.

The echo-top height, which is discretized on a 1 km vertical grid, is defined in *Cooney et al.* (2018) as the highest altitude in each column with $Z_H \geq R_1$, with the additional constraint that the reflectivity in the altitude bin closest to the tropopause must be greater than or equal to a second threshold R_2. The second condition serves to filter spurious above-tropopause echoes. *Cooney et al.* (2018) uses $R_1 = 10$ dBZ and $R_2 = 20$ dBZ. These thresholds remove potentially false identifications but could also miss some OTs. To evaluate the sensitivity of the retrievals to the choice of reflectivity thresholds, four sets of criteria are used here, listed in Table 5.1. Two options omit the R_2 criterion. Unless explicitly noted, OTN in this paper refers to NEXRAD overshoots using criteria 1 (i.e., the *Cooney et al.* (2018) criteria).

2.3 *Bedka and Khlopenkov* (2016) GOES OT Analysis (Version 1)

GOES retrievals of OTs are made using the IR-texture method described in *Bedka and Khlopenkov* (2016). Similar to the NEXRAD analysis, an individual GOES OT is defined as a contiguous group of GOES pixels identified as overshooting. Information about each overshoot includes the estimated parallax correction, the minimum brightness temperature (T_b), the difference between the minimum cloud top T_b and tropopause temperature ($\Delta T_{MERRA} = T_b - T_{MERRA}$), the OT probability, the difference between the minimum cloud top T_b and the most unstable level of neutral buoyancy temperature (IR-most unstable equilibrium level), and the difference between the minimum cloud top T_b and the anvil-mean T_b (IR-anvil BTD). Here, most unstable refers to the parcel that yields the highest convective available potential energy in the layer 0-3 km above ground level. Parallax correction values are applied to each anvil location and are based on a constant 14 km altitude. Because parallax correction values are applied to only the anvil regions and high clouds can block the field of view, GOES OT Version 1 data maps can have 'gaps' of missing information near some storms. The GOES data are produced on a $\sim$4 km horizontal grid for each GOES scan within the region from $\sim$128°W–61°W and $\sim$21°N–56°N, but only data located within the

NEXRAD analysis domain are used in this study.

OT probability values are assigned to potential OT candidates using a logistic regression approach. The primary inputs to the logistic regression include IR-anvil BTD (∼70% of weight), ΔT_{MERRA} (∼13.7% of weight), and IR-most unstable equilibrium level (∼1.6% of weight). The remaining weight is based on shape correlation because OTs are expected to be circular or elliptical. OT probabilities range from 0 (not an OT) to 1 (definitely an OT). Using a probability threshold that is too low results in a higher rate of falsely identified OTs and includes events that overshoot the anvil but not the tropopause, while a threshold that is too high causes the algorithm to miss tropopause-overshooting events. For the purposes of this study and in an attempt to exclusively retain tropopause-overshoots, only OT probabilities ≥ 0.7 are used. This value was chosen based on personal communication with the authors of *Bedka and Khlopenkov* (2016), regarding our research objectives.

Table 2.1: GOES OT file dates

Month and Year	Day
June 2004	9, 10, 11, 12, 13, 14, 15, 16, 17, 18, 19, 20, 21, 22
April 2006	7, 8
May 2006	5, 6
June 2006	10, 11, 12, 13, 14, 15, 16, 17, 18, 19, 20, 21, 22, 23

2.4 Revised GOES OT Analysis (Version 2)

GOES retrievals of OTs are also made using a revised version of the *Bedka and Khlopenkov* (2016) IR-texture method. The GOES Version 2 OT detection scheme is designed to be near-real time and work everywhere in the world. IR-most unstable equilibrium level, the third largest contributor to the logistic regression equation used to calculate OT probability in Version 1, is not

used in the revised analysis. In many locations, little information is available about the boundary layer structure, which causes the equilibrium level metric to be unreliable. In addition, the metric takes some time to compute, which increases latency for real-time applications, so it is not used in the Version 2 algorithm.

Parallax correction values are applied to each point in the domain based on a constant 15 km altitude so that all pixels are moved uniformly and there are no gaps in the storms. This differs from Version 1, in which a 14 km correction is applied only to the anvil. The use of a constant parallax-correction altitude is a reasonable approximation for mid-latitude convection because GOES navigation wobble (which can exceed 4 km from image to image, especially with older GOES satellites), observing-time differences between satellite and radar, and other factors introduce comparable errors. Using NEXRAD z_e data, the horizontal displacement error of an OT resulting from assuming a constant parallax-correction altitude is found to range from -2 to +8 km, with an average of $\sim +4$ km, which corresponds to about 2 GridRad grid boxes. Positive values indicate that the echo-top altitude is less than the assumed value of 15 km. Due to the seasonal evolution of the tropopause over the CONUS, a correction of 15 km is likely more accurate in July and August than the months used in this study (April, May, and June).

One significant change in Version 2 (V2) from Version 1 (V1) is the manner in which the anvil is identified. Recall, OT candidates are compared to the anvil mean temperature in order to calculate the OT probability. In Version 1, *Bedka and Khlopenkov* (2016) first finds an OT candidate and then calculates the mean anvil temperature from surrounding pixels. An issue arises when two OT candidates are located within very close proximity to one another. For these cases, IR T_b of the nearby OT candidate is included in the mean anvil temperature calculation, biasing the anvil cold. In the revised method, the anvil is identified by first calculating an anvil cloud likelihood score that is derived from spatial testing and a comparison against the MERRA-2 tropopause. Once the anvil is identified, it is searched for potential OT candidates. If two or more OT candidates are still in close proximity, the more prominent candidate is retained and the other is eliminated.

Another issue with *Bedka and Khlopenkov* (2016) is that the IR-anvil BTD is unrealistically

large in situations with somewhat broken anvil cloud. The broken anvil cloud biases the anvil calculation warm, relative to the OT candidate. This gives the illusion that the OT candidate is much colder than its surroundings. In response, the Version 2 method changes how weights are fed into the logistic regression equation. Rather than using fixed weights for each parameter, as is the case in *Bedka and Khlopenkov* (2016), the new method applies an approach similar to fuzzy logic. Fuzzy logic is a process that is based on assigning variables values or 'degrees of truth', ranging from 0, definitely not true, to 1, definitely true. Values in between 0 and 1 show the confidence that something is true. For example, a score of 1 is given if the IR T_b is 5 K colder than T_{MERRA2} ($\Delta T_{MERRA2} = T_b - T_{MERRA2}$). In the revised OT detection methods, the authors allow for events with ΔT_{MERRA2} colder than 5 K to receive 'bonus points' in the fuzzy logic computation. The bonus points allow the confidence score to reach as high as 2 and are given for this metric because an event with T_b that much colder than the tropopause is almost certainly an OT, despite what other parameters might suggest. For IR-anvil BTD, a maximum score of 1 (0.6) is given if the T_b of a pixel is 8 K (5 K) colder than the anvil. There are no bonus points given for this metric because warm temperature pixels can sometimes be included in the anvil mean computation of a small anvil area, resulting in unrealistically high IR-anvil temperature differences. Truth value scores are accumulated and the end result is a 0-1 OT probability as before. In addition to the ΔT_{MERRA2} and IR-anvil BTD, the OT probability equation takes into account the area of cold cloud surrounding a pixel and spatial coherence of the anvil. As with Version 1, only Version 2 OT probabilities ≥ 0.7 are used.

3. HYPOTHESES

In this study we evaluate eight possible sources of disagreement between the NEXRAD and GOES retrieval methods in detecting tropopause-overshooting convective events:

1. The MERRA and ERA-I tropopause analyses used by the GOES and NEXRAD methods, respectively, may be biased with respect to each other, leading to systematic differences in OT detection.

2. Radar coverage is sparse in some regions, which could cause NEXRAD overshoot detection failures.

3. The NEXRAD OT method may underpredict the quantity and size of overshooting echo due to a limited sensitivity to small particles.

4. The GOES OT method may identify updrafts colder but below the tropopause as overshoots due to the ambiguity in the relationship between temperature and altitude.

5. The GOES OT method may falsely identify events as overshoots in stratiform regions because the IR-anvil brightness temperature difference (IR-anvil BTD) is unrealistically high in situations with broken anvil cloud.

6. The GOES algorithm may identify above-anvil cirrus cloud as OTs.

7. The GOES OT method may identify updrafts that overshoot the anvil but not the tropopause due to how weighting of metrics in the logistic regression equation attempts to address the ambiguity in the relationship between temperature and altitude.

8. The GOES OT method may miss tropopause-overshooting events because the brightness temperature is warmer than the tropopause as a result of stratospheric mixing.

To test these hypotheses we analyze all tropopause-overshooting storms identified by the two observing systems in the eastern two-thirds of the United States for selected dates in 2004 and 2006 that have active convection. The dates are listed in Table 2.1.

4. METHODS

4.1 Temporal Matching of NEXRAD and GOES Analyses

NEXRAD analyses are generated hourly on the hour by merging all available radar scans within a ± 3.8 minute analysis window centered on the nominal analysis time. During the study period, the Geostationary Operational Environmental Satellite-12 (GOES-12) provided imagery of the CONUS at approximately 15-minute intervals, although the scanning schedule was not completely uniform. GOES-12 begins scanning the NEXRAD analysis region 2.4 minutes after the hour and requires $\sim$2.9 minutes to scan the full region. Due to the CONUS scan strategy, some hourly NEXRAD analyses do not have matching GOES images, particularly 0300, 0600, ..., 2100 UTC. Here we use GOES Version 1 and 2 overshoot analyses from 500 matching GOES CONUS images. To evaluate the impact of the timing difference between the NEXRAD and GOES analyses, additional GridRad analyses, centered at 3 minutes after the UTC hour, are computed for a subset of the analysis times.

4.2 Spatial Matching

Spatial matches between individual GOES and NEXRAD overshoots are identified by mapping the GOES data to the GridRad grid using the estimated parallax corrections. The GOES-12 IR data grid has approximately half the resolution of the GridRad grid in each dimension, so each GOES pixel is mapped to the four GridRad grid boxes nearest to the parallax-corrected pixel location. If multiple GOES pixels are mapped to the same GridRad grid box, the GOES data values are averaged. For regions with pixels identified as GOES OTs, only the overshoots, with detection probabilities ≥ 0.7, are included in the averaging. This is done to preserve the overshoot data and avoid contamination by surrounding pixels that are not part of an overshoot but are parallax corrected into the same grid box.

Because the GOES overshoot algorithm is applied to the original (non-parallax-corrected) GOES images, the parallax corrections cause some spatially distinct GOES OTs to be contiguous with one

another when mapped to the GridRad grid. In this case, the GOES OTs are combined into a single overshoot. Contiguous GOES overshoots, on the GridRad grid, with detection probabilities ≥ 0.7 are denoted OTG in this paper. OTG and OTN that overlap in one or more GridRad grid box are considered to be co-located. It is important to note that more than one OTG can overlap an OTN and vice versa. Therefore, the total number of OTG co-located with OTN is not always equivalent to the total number of OTN co-located with OTG. OTG from the original *Bedka and Khlopenkov* (2016) IR OT algorithm (V1) and revised IR OT algorithm (V2) are referred to as OTG_1 and OTG_2, respectively.

Due to its lower horizontal spatial resolution, the GOES analysis is unlikely to be able to detect very small-scale overshoots that may be observable by NEXRAD. To remove instrumentation differences and ensure a consistent comparison, only OTG and OTN that contain at least 5 GridRad grid boxes are included in this analysis. For the 500 temporal matches, the NEXRAD method finds 3404 OTN that are at least 5 grid boxes in size. There are 12265 OTG_1 and 4272 OTG_2 that contain at least 5 GridRad grid boxes.

4.3 Removing Low Radar Coverage Regions

The GOES satellite can image the entire study region with relatively uniform coverage, but the NEXRAD network has a complex, time-dependent coverage pattern (*Cooney et al.*, 2018). Figure 4.1 shows the average number of contributing NEXRAD radar azimuth scans per analysis time within each grid column in the domain. Coverage is good in the plains, midwest, and southeast regions of the United States. Therefore, differences in overshoot detections in the southeast US cannot be attributed to limited radar coverage. Coverage in the western US (where there are fewer radars), offshore, and outside international borders, is generally poorer; and the likelihood of NEXRAD detecting an overshooting event is lower. *Homeyer* (2014) shows that the achieved vertical resolution is ≤ 1 km if at least three radars observe a column. When precipitation is present, this corresponds to $\sim$40 radar azimuth scans. Therefore, the OTG/OTN comparison is only done in locations with ≥ 40 NEXRAD instantaneous radar azimuth scans in a column. Of the 3404 OTN

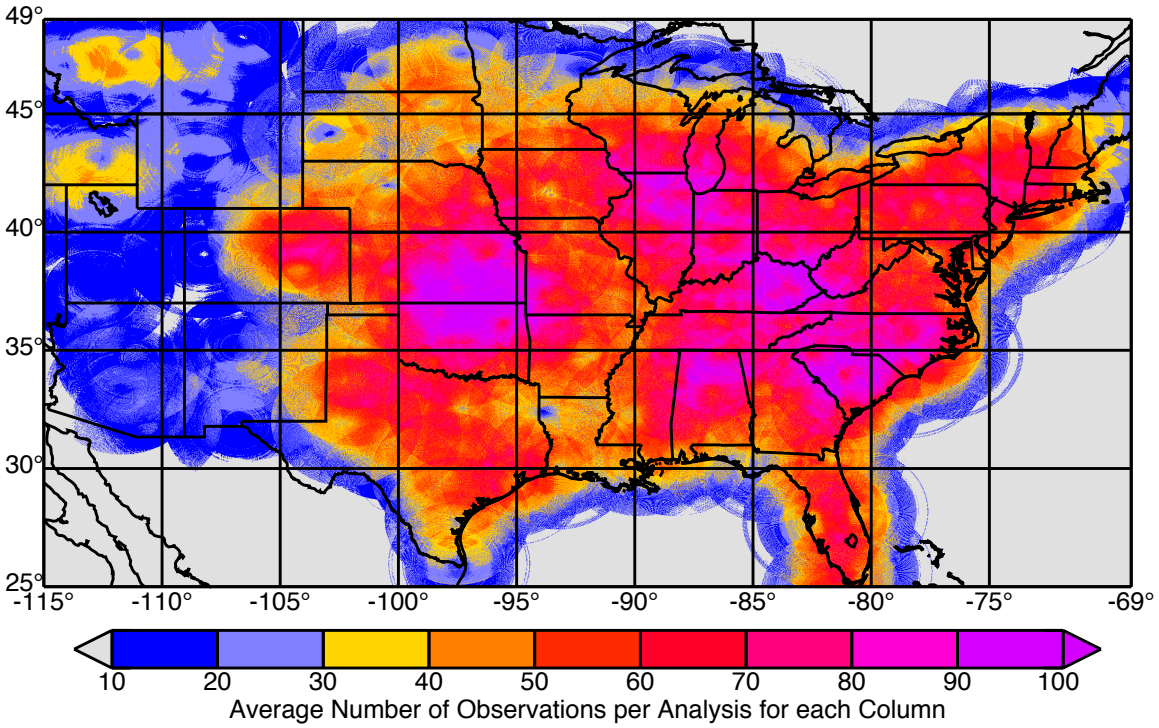

Figure 4.1: Average number of contributing NEXRAD radar observations per analysis time within each GridRad grid column during the analysis dates listed in Table 2.1. Locations with gray color fill correspond with no or very few contributing NEXRAD radar observations, while locations colored blue are indicative of inadequate radar coverage for reliable overshooting analysis.

that are at least 5 grid boxes in size, 3120 meet that criterion. In addition, 9795 OTG_1 and 3711 OTG_2 satisfy that criterion.

4.4 Case Studies

To understand the reasons for the differences between the three methods, a number of individual analysis times were selected for detailed study. To determine which dates and regions to analyze, OTG_1, OTG_2, and OTN are mapped for each of the 500 analysis times. In order to test the hypotheses, case study regions are chosen based on 4 factors. First, OTG_1 and OTG_2 are both mapped to observe how changes to the GOES algorithm by the revised method impacts the OT identifications. Second, we include regions in which OTG and OTN overlap to observe how those events differ from OTG and OTN that do not overlap. Third, we chose regions in which OTG are observed but OTN are not. For this, we made sure to include events in the southeast US in order

to determine why there are major OT detection differences there. Lastly, we chose regions where OTN are identified but OTG are not in order to investigate why the OTG method does not observe the OT. After reviewing every hourly map, 10 analysis times are selected for further analysis. These analyses contain 25 storm subregions of interest. Table 4.1 list the case study times chosen. Each storm subregion is referred to as a case.

Table 4.1: Case Study Analysis Times

2004-06-09-01Z	2004-06-09-02Z	2004-06-09-04Z	2004-06-14-23Z	2004-06-15-08Z
2004-06-16-22Z	2006-04-08-20Z	2006-05-06-01Z	2006-06-12-19Z	2006-06-22-20Z

Case study overshoots are evaluated by visually inspecting NEXRAD tropopause-relative echo-top height (z_r) maps, vertical reflectivity cross sections, parallax corrected IR T_b maps, parallax corrected IR-anvil BTD maps, parallax corrected IR-tropopause temperature difference maps, T_{ERA} subtracted from T_{MERRA} and T_{MERRA2} maps, OT probability maps, and composite reflectivity maps.

5. RESULTS

5.1 Geographic Distribution of Overshoots

Figure 5.1 displays the overshoot locations for each OT identification method during the study dates. As expected from previously published results, GOES V1 identifies far more OTs than NEXRAD, particularly in the southeast US. The spatial distributions of GOES V2 and NEXRAD agree much better, although V2 finds more (3711 vs. 3120) and larger OTs than NEXRAD. OTN, OTG_1, and OTG_2 contain an average of 30.7, 36.9, and 72.2 GridRad grid boxes (not shown), respectively.

For comparison with Figure 5.1b, Figure 5.1d shows the difference between OTG_1 occurrences when the radar azimuth scan threshold is not applied and panel b overshoot detections. Over the southeast US, OTG_1 differences are small, indicating that radar coverage is not the reason for the smaller number of OTN relative to OTG_1 there. In the western US, where OTN identifications are rare and the radar coverage is also poor, there are few OTG_1 and OTG_2, which indicates that there are, in fact, few OT occurrences there.

5.2 Matching Statistics Overview

Section 1 of Table 5.1 shows the co-location statistics for OTG_1 events from *Bedka and Khlopenkov* (2016) and OTN events from *Cooney et al.* (2018). In total, over 3 times as many OTG_1 are identified as OTN. Approximately 40% of the OTN are co-located with OTG_1, but only about 13% of the OTG_1 are co-located with OTN. When comparing OTG_1 with NEXRAD OT analyses centered at 3-minutes after the UTC hour (not shown), the fraction of overshoot matches increases by only $\sim$1-3%, indicating timing differences have only a small impact on the comparisons. The small fraction of matches for both analyses suggests that the NEXRAD analysis is failing to detect OTs, the OTG_1 analysis is erroneously identifying OTs, the matching criteria are too stringent, or a combination of those factors.

Table 5.2 shows the co-location statistics for OTG_2 and OTN events. Results are shown for

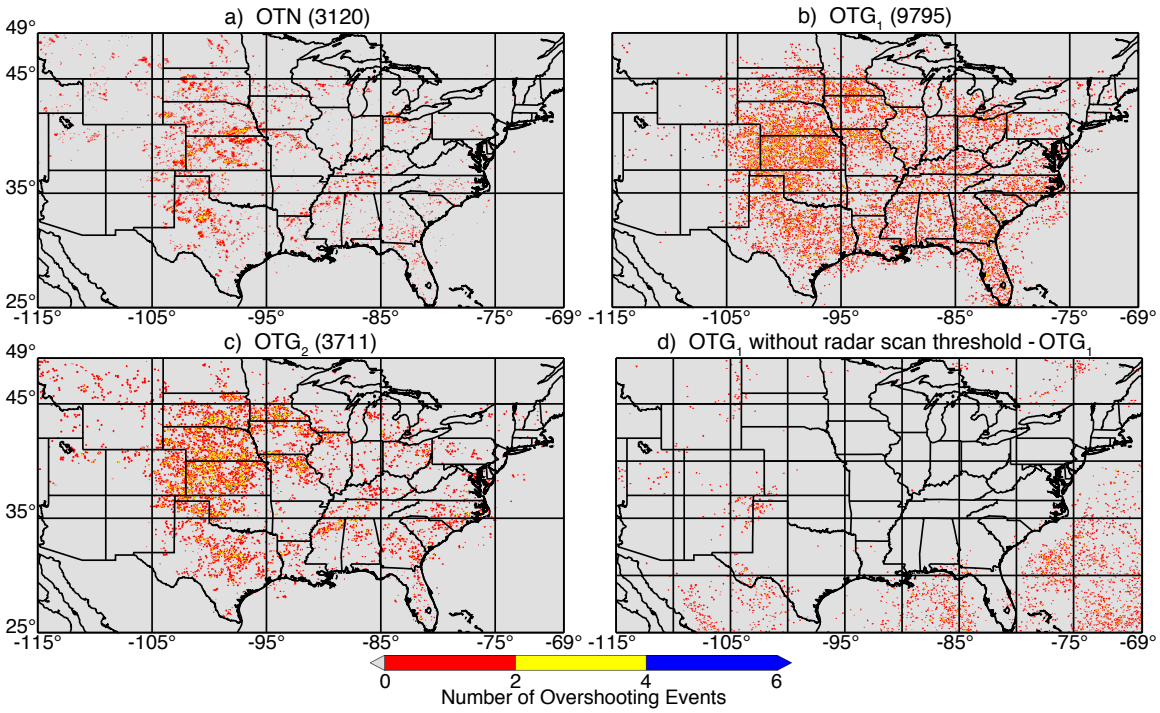

Figure 5.1: Number of instances in the selected analyses that overshooting convection is identified for each GridRad pixel. The number in the parentheses of each map is the total number of overshooting events identified by the respective methods. (a) OTN. (b) OTG_1. (c) OTG_2. Panels a, b, and c include only pixels where the number of radar azimuth scans observing a grid column ≥ 40. (d) OTG_1 with no radar azimuth scan threshold applied minus Panel b.

Table 5.1: Number of OTG_1 and OTN co-located and not co-located with one another for each OTN criteria. R_1 and R_2 represent the 2 reflectivity thresholds used to identify OTN. The $+$ and $-$ signs indicate co-located and not co-located overshoots, respectively.

		NEXRAD Criteria (dBZ)		Overshoot Count			
		R_1	R_2	TOTAL	$+$	$-$	% Matches
1)	OTN	10	20	3120	1246	1874	39.9%
	OTG_1			9795	1297	8498	13.2%
2)	OTN	5	20	3207	1275	1932	39.8%
	OTG_1			9795	1338	8457	13.7%
3)	OTN	10	N/A	5593	1805	3788	32.3%
	OTG_1			9795	2009	7786	20.5%
4)	OTN	5	N/A	7405	2085	5320	28.2%
	OTG_1			9795	2551	7244	26.0%

different spatial matching criteria. A distance of 0 km indicates that the OTs must overlap, which is the criterion used in Table 5.1. The revised GOES analysis contains only ∼38% as many detections as the original analysis, which is much closer to the number of OTN, but both overall match rates are still under 50%. The fraction of OTG_2 that match OTN is double that of OTG_1, but the number of OTN matches is somewhat smaller. This suggests that some OTG_1 and OTN matches are not identified by the revised GOES overshoot detection scheme.

Even though OTG_2 are often much larger than OTG_1 and OTN, it is rare for an OTN to be co-located with an OTG_2 if it is not also co-located with an OTG_1 (∼9% of time). Only ∼30% of OTG_1 have at least one GridRad grid box in common with an OTG_2, while ∼70% of OTG_2 overlap an OTG_1 (not shown). This suggests that the improvement in co-location frequency is not a product of the OTG_2 being larger and simply 'absorbing' smaller, non-co-located OTG_1. Instead, as will be shown, the revised GOES method removes many OTG_1 'false positives' but finds almost no new 'correct positives'. Why the average OTG_2 is much larger than OTG_1 is unknown and may be a topic of discussion in future research.

5.3 Tropopause Biases

Tropopause differences between ERA-I, MERRA, and MERRA-2 could lead to systematic biases in OT detections. To evaluate whether biases in the tropopause analyses are responsible for

Table 5.2: Number of OTG_2 and OTN co-located and not co-located with one another at set distances. The $+$ and $-$ signs indicate OTG_2/OTN that overlap an OTN/OTG_2 within the specified distance and overshoots that do not overlap within those distances, respectively.

		Overshoot Count			
	Distance (km)	TOTAL	$+$	$-$	% Matches
OTN	0	3120	1068	2052	34.2%
OTG_2		3711	995	2716	26.8%
OTN	5	3120	1285	1835	41.2%
OTG_2		3711	1186	2525	32.0%
OTN	10	3120	1483	1637	47.5%
OTG_2		3711	1375	2336	37.1%
OTN	25	3120	1774	1346	56.9%
OTG_2		3711	1735	1976	46.8%

the differences between the NEXRAD and GOES OT results, Figures 5.2a, b, and c compare the tropopause temperatures from MERRA, MERRA-2, and ERA-I across the study domain during the 500 matching analysis times. Because OTs cool at a rate of 7-9 K/km as they ascend into the lower stratosphere (*Bedka et al.*, 2010; *Negri*, 1982; *Adler et al.*, 1983; *Griffin et al.*, 2016; *Smith et al.*, 2017), a difference of 4 K in the UTLS corresponds to $\sim$0.5 km. MERRA and MERRA-2 tropopause temperatures are within 4 K of each other $\sim$84% of the time, with MERRA-2 colder on average than MERRA. This suggests the MERRA-2 tropopause is higher on average, and the likelihood of identifying an OT is reduced. The MERRA-2 tropopause temperature, used in the OTG_2 method, also agrees better with the ERA-I tropopause temperature than the MERRA tropopause temperature (panels a and c).

Occasionally, similar tropopause *temperatures* can be identified at very different *altitudes*. Large tropopause differences ($>$ 2 km) are most often due to a failure of one of the analyses to detect the primary tropopause in double tropopause locations. This most often occurs near the tropopause break associated with the subtropical jet. Figures 5.2c and 5.2d show generally good agreement for temperature but poor agreement for altitude between ERA-I and MERRA-2. Here, Z_{MERRA2} is often much higher than Z_{ERA}, demonstrating that MERRA-2, which is used in the OTG_2 method, is missing primary tropopauses identified in ERA-I. As will be shown in the next few paragraphs,

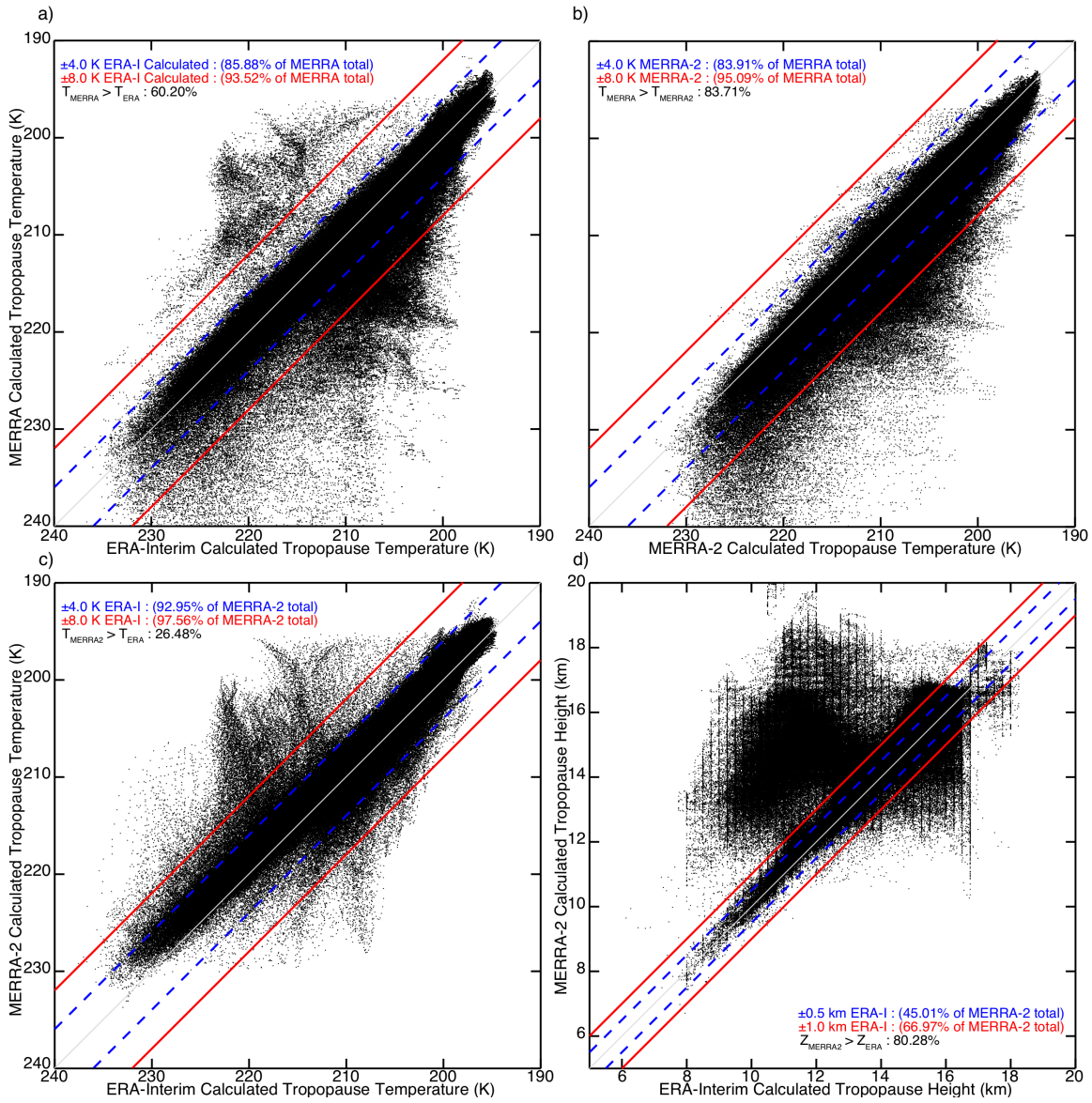

Figure 5.2: Comparison for all analysis times of tropopause (a) temperatures from ERA-I and MERRA, (b) temperatures from MERRA-2 and MERRA, (c) temperatures from ERA-I and MERRA-2, and (d) altitudes from ERA-I and MERRA-2. Note that the temperature scales are reversed. Points between the solid red and dashed blue lines in a-c are values that agree within ±8 K and ±4 K, respectively. Points between the solid red and dashed blue lines in d are values that agree within ±1.0 and ±0.5 km, respectively. Labels display the frequency with which those instances are observed.

the calculation of the tropopause on an irregular vertical grid by the OTG_2 method causes the tropopause altitude differences. It is important to emphasize that the MERRA-2 tropopause used for the OTG_2 retrievals is calculated from MERRA-2 geopotential height, pressure, and temperature data as part of the OTG_2 processing algorithm. This is *not* the MERRA-2 tropopause product distributed as part of the reanalysis. Also, the raw MERRA-2 data are *not* the reason the OTG_2 method misses the primary tropopause here. It is the calculation of the tropopause by the OTG_2 method.

Figure 5.3 provides an example of an OTG_2 identified in a double tropopause region. Here, the MERRA-2 primary tropopause altitude (horizontal blue line in Figure 5.3c and d) is at the same altitude as the ERA-I model secondary tropopause altitude (horizontal light orange line in Figure 5.3c). The black line in panel d shows the ERA-I temperature profile. The blue and orange circles in panel d show the MERRA-2 and ERA-I primary tropopause temperatures, respectively. The blue circle is not exactly aligned with the ERA-I temperature profile due to small differences between the temperature profiles. Although the primary tropopause temperatures differ by only a few Kelvin, the heights differ by $\sim$4 km. Here, the ERA-I data shows a strong inversion in the layer ($\sim$7 K) 1-2 km above the primary tropopause, with a less stable layer above. In our analysis, as explained in the next paragraph, we find that the primary tropopause is missed in the OTG_2 method because the OTG_2 method calculates the tropopause on an irregular altitude grid and incorrectly applies the definition of the tropopause.

Recall, the World Meteorological Organization (WMO) defines the primary lapse-rate tropopause as the lowest level at which the lapse-rate decreases to 2 K/km or less, provided also the average lapse-rate between this level and all higher levels within 2 km does not exceed 2 K/km (*WMO*, 1957). When the tropopause is calculated in the OTG_2 method, the lowest level at which the lapse-rate decreases to at least 2 K/km is first found and then the lapse-rate for the next 2 *model vertical pressure levels* is calculated to determine if it exceeds 2 K/km. The OTG_2 method lapse-rate calculation does not ensure the 2 adjacent pressure levels are within 2 km and calculates the lapse-rate between each pressure level, rather than computing the average. For the example in Figure 5.3 and

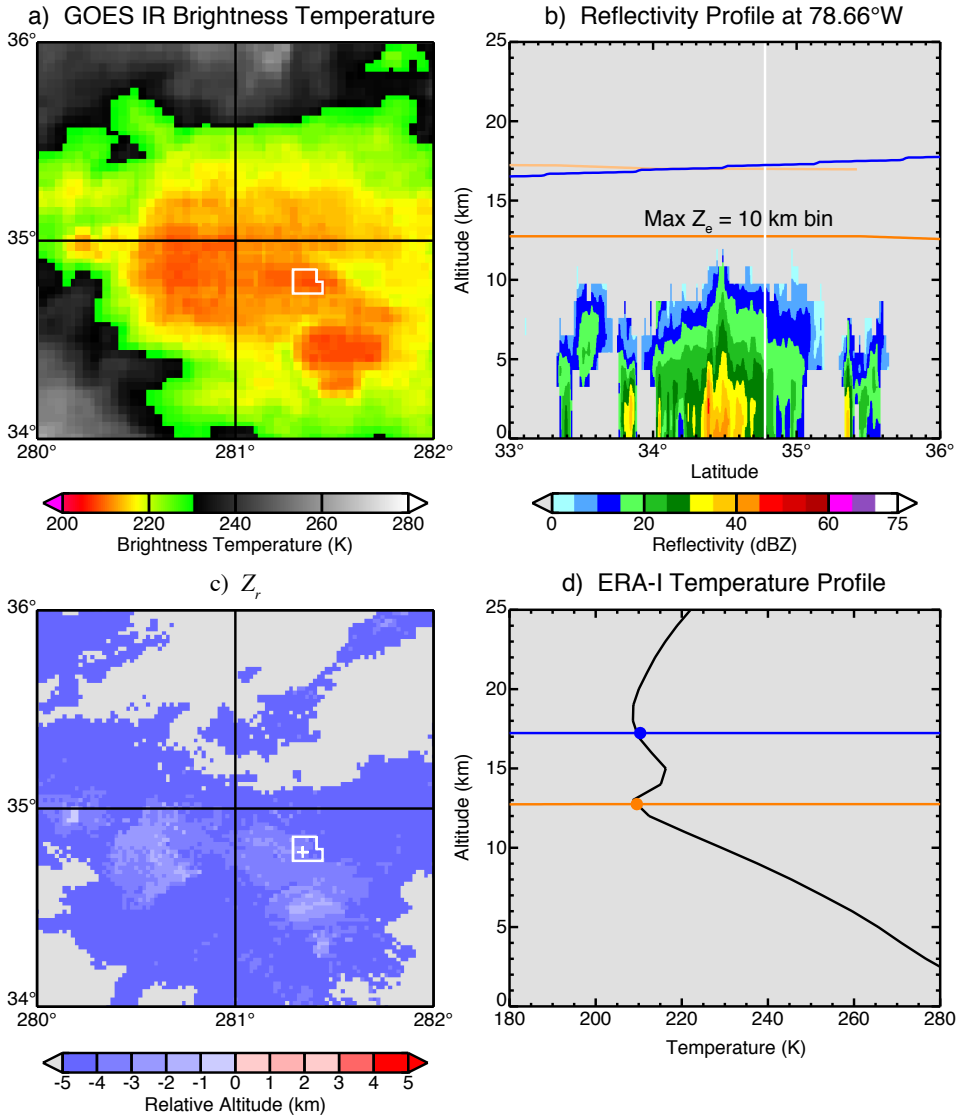

Figure 5.3: Analysis for 6 May 2006 at 0200Z. (a) Parallax corrected IR T_b map. White box outlines OTG_2 of interest location. (b) Latitude-altitude reflectivity cross-section through the middle of the OTG_2. Center of OTG_2 is marked by the vertical white line. The horizontal orange and light orange lines indicate the ERA-I primary and secondary tropopause heights. The horizontal blue line indicates Z_{MERRA2}. (c) NEXRAD 10 dBZ z_r map. White crosshair marks the middle of the OTG_2 and white box outlines the OTG_2 location. (d) ERA-I temperature profile through the middle of the OTG_2. The horizontal orange and blue lines show the primary ERA-I and MERRA-2 tropopause height, respectively. The orange and blue circles mark T_{ERA} and T_{MERRA2}, respectively.

others like it, the stable layer is not deep enough to capture the primary tropopause when calculated in this manner. The GOES method can easily fix this issue by only using temperature data located within 2 km, rather than 2 pressure levels, of a potential tropopause and computing the average lapse-rate within the 2 km. We obtained a subset of MERRA-2 raw data and calculated the tropopause following the WMO definition. We also obtained a subset of MERRA-2 tropopause data products, available from NASA. These tropopause altitudes and temperatures closely match Z_{ERA} and T_{ERA}. Approximately 95% of tropopause altitudes agree within $\pm$1 km and the MERRA-2 tropopause is identified at a higher altitude than Z_{ERA} only $\sim$60% of the time (not shown). Therefore, the issue is with how the OTG_2 method calculates the tropopause, *not* with the MERRA-2 data. Because the OTG_2 method is based on tropopause temperature and the secondary tropopause temperature is often nearly the same as the primary tropopause temperature in double tropopause regions, we found the incorrect tropopause identification has little impact on the co-location frequency between the GOES and NEXRAD detection methods. However, in the case study analysis, we did observe a few instances in which the identification of OTs is impacted by large tropopause differences, unrelated to the GOES method missing the primary tropopause.

5.4 Comparison of NEXRAD and GOES V1

5.4.1 Dependence on NEXRAD Overshooting Criteria

Cooney et al. (2018) applies strict echo top criteria in order to avoid false positives that occur when the reflectivity threshold nears the noise limit of the NEXRAD radars. To evaluate whether the differences between NEXRAD and GOES V1 are due to overly strict NEXRAD detection criteria that fail to detect overshooting tops, we compute co-location fractions using relaxed NEXRAD criteria (Table 5.1) that range from most restrictive (1) to least restrictive (4). In these comparisons the number of OTG_1 remains the same, while the number of matches changes. Unsurprisingly, as the detection criteria are relaxed, the number of NEXRAD overshoots increases from 3120 (criteria 1) to 7405 (criteria 4), and the percentage of OTG_1 matches with OTN increases from 13.2% to 26.0%. At the same time, however, the percentage of OTN matches falls from 39.9% to 28.2%,

which suggest that the number of false positives increases more than the number of correct positives. This is consistent with the echo detection limits for the NEXRAD radar system. NEXRAD radars have a limited sensitivity to small particles. A lower echo top threshold can provide a better estimate of the true top altitude, however, it also introduces more noise. The nominal reflectivity threshold for the existence of a valid echo is $\sim$5 dBZ, but at the maximum range used for the merging of multiple radars, the minimum detectable signal is $\sim$7.5 dBZ (*Cooney et al.*, 2018). It is not surprising that false positives increase when the detection threshold approaches the sensitivity limit of the radars, and overall relaxing the NEXRAD OT criteria does not improve the frequency of agreement with OTG_1.

5.4.2 GOES V1 Overshoots Colder than Tropopause but do not Surpass it

One possible source of GOES retrieval errors is identifying updrafts with cloud tops colder but below the tropopause as overshooting tops. This can occur when an updraft rises and cools faster than the upper tropospheric environment. To evaluate this possibility, we review case study storms. Figure 5.4a shows an example case. Each OTG_1 in the case is plotted on the corresponding composite reflectivity map. The red shading on the map shows the locations of strong updrafts (composite reflectivity $\geq$ 45 dBZ). For this case, 8 of the 15 OTG_1 are located within these updraft regions (OTG_1 82, 85, 86, 87, 89, 90, 95, and 96). The white identification numbers correspond to OTG_1 that are co-located with OTN, all of which are observed within strong updrafts. Not all OTG_1 observed within strong updrafts are co-located, however. Radars observe echo $\sim$0.5 km above Z_{ERA} in parts of the OTG_1 82 and 86 regions, however, there are not at least 5 contiguous GridRad overshooting pixels. A time series analysis of this region shows these OTG_1 are growing and become OTN 5 minutes after the analysis time. This suggests OTG_1 82 and 86 are likely missed due to timing differences.

OTG_1 numbers 87 and 90 are located in a region in which $T_{ERA} < T_{MERRA2} << T_{MERRA}$ and 10 dBZ $z_r \simeq$ -1 km. Due to the tropopause temperature differences, the cloud top IR T_b of OTG_1 90 is entirely warmer than T_{ERA} while $\sim$50% of OTG_1 87 is warmer than T_{ERA}. OTG_1 95 is located

where $z_r \simeq$ -0.25 km but T_{ERA} is 3 K colder than T_{MERRA}. Here, the ERA-I model estimates the upper troposphere lapse-rate to be approximately -6 K/km and the OTG_1 95 cloud top is $\sim$5 K colder than T_{ERA}. Because OTs rise and cool 7-9 K/km as they ascend into the lower stratosphere (*Bedka et al.*, 2010; *Negri*, 1982; *Adler et al.*, 1983; *Griffin et al.*, 2016; *Smith et al.*, 2017), these instances suggest either tropopause differences or updraft tops colder than the environment might be causing the OT detection differences. For OTG_1 95, it is also possible that the NEXRAD method misses an overshoot there because the radars are not sensitive to particles smaller than precipitable hydrometeors. This scenario is possible for this OT identification because the radars observe echo very near Z_{ERA} while the MERRA and ERA-I tropopause temperature differences are small. While we know it is possible for cloud tops to be colder than the tropopause but not actually overshoot it, we are unable to definitively determine the cause of the detection difference in this case due instrument limitations and the ambiguity in the relationship between temperature and altitude.

Figure 5.5 shows a histogram of the maximum reflectivity within co-located and not co-located OTG_1. The co-located OTG_1 are nearly always located within strong updraft regions. Quite a few OTG_1 are located within strong updraft regions but are not co-located, however. This suggests the NEXRAD criteria are too strict in some places or those GOES V1 identifications are identified within updrafts but the tops do not surpass the tropopause.

5.4.3 GOES V1 Overshoots in Stratiform Regions

Another possible source of GOES retrieval errors is identifying cold anvil cloud as an overshooting top. Nearly half of the OTG_1 in Figure 5.4a are identified outside of strong updraft regions. Similar results are observed in other cases not shown. Some OTG_1 are not located near a strong updraft, such as OTG_1 88 and 91, while others are slightly displaced from strong updrafts (OTG_1 83, 84, 92, and 94). OTG_1 88 may be part of a weaker updraft but the top is entirely warmer than T_{MERRA} ($\Delta T_{MERRA} > 0$). Therefore, this is likely a bad GOES V1 tropopause-overshoot identification. OTG_1 91 is located on the edge of the observed reflectivity region. Figure 5.4d shows very warm IR T_b nearby and GOES visible imagery shows broken anvil cloud adjacent to

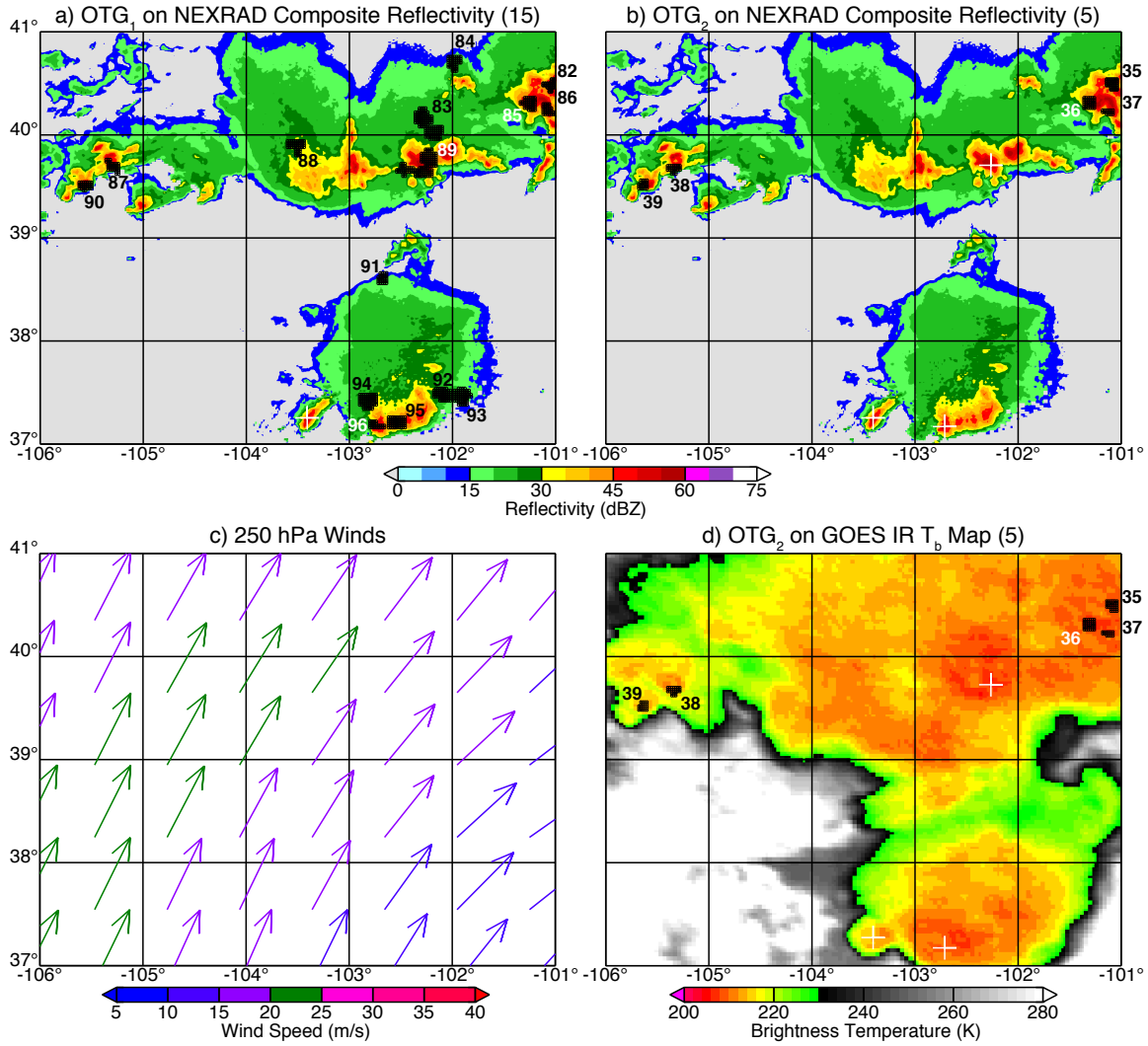

Figure 5.4: Example NEXRAD composite reflectivity map used to evaluate case study overshooting events. This example is from 9 June 2004 at 0200Z. a) The reflectivity is indicated by the shaded colors. The open black circles indicate OTG_1 pixels. The numbers nearby the OTG_1 serve as an identification number. White identification numbers correspond to OTG_1 that are co-located with an OTN. White crosshairs show OTN locations that are not co-located. The number inside of the parentheses corresponds to the number of OTG_1 observed in the case. b) Same as Figure 5.4a but for OTG_2. c) Map of 250 hPa winds. The arrows point in the direction of the wind. The magnitude of the speed is indicated by the color shading. d) Same as Figure 5.4b but parallax-corrected GOES IR brightness temperature (T_b) is indicated by the shaded colors.

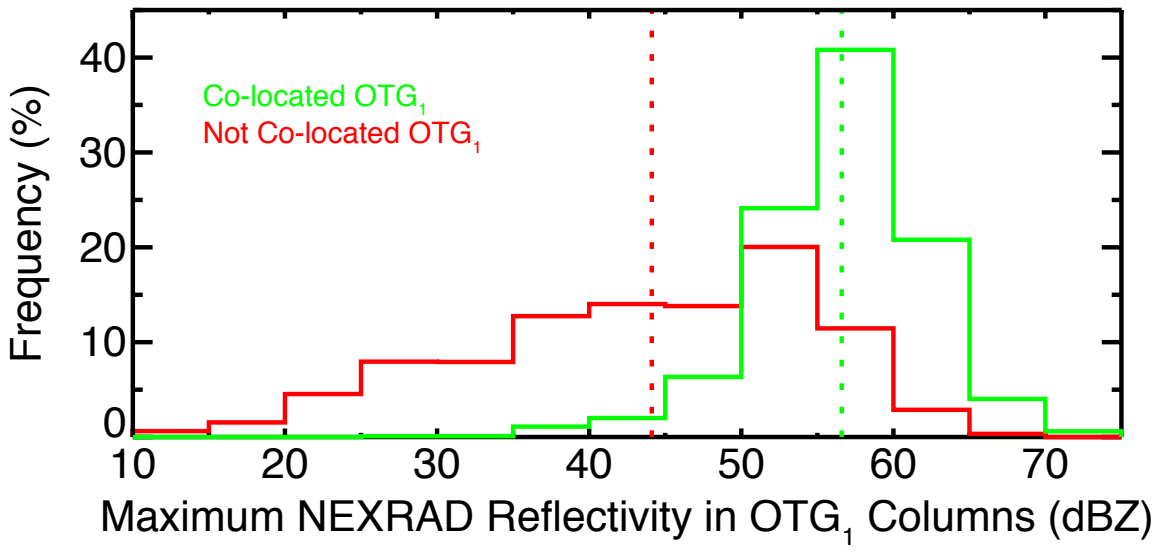

Figure 5.5: Histogram of maximum reflectivity within OTG_1. The solid green and red lines indicate co-located OTG_1 and not co-located OTG_1, respectively. The corresponding colored dashed lines provide the respective median values.

the OTG_1 identification (not shown). The broken anvil biases the IR T_b of the anvil warm and thus the horizontal temperature gradient around OTG_1 91 is artificially large. Thus, this is a situation in which the IR-anvil BTD is larger than it should due to broken anvil cloud.

OTG_1 located near updrafts and overshoots may be a result of injected cirrus that cannot be observed by the NEXRAD radars. IR satellite imagery often identifies a distinct cold "V" feature at the cloud top of some tropopause-penetrating thunderstorms (*Adler et al.*, 1981; *Fujita*, 1982; *Negri*, 1982; *Homeyer*, 2014). The most likely mechanism for their formation is above-anvil (stratospheric) cirrus clouds (*Homeyer*, 2014). To determine if any of these OTG_1 are above-anvil cirrus, the ERA-I 250 hPa winds in Figure 5.4c are provided as a complement to Figure 5.4a. Figure 5.4c shows the 250 hPa winds are blowing towards the northeast, which may account for OTG_1 83 and 94. OTG_1 83 is directly northeast of an updraft in which another OTG_1 is co-located with an OTN. It is possible anvil material is lofted immediately downstream of the overshooting top via gravity wave breaking. OTG_1 94 is located north of a strong updraft that contains an OTG_1 co-located with an OTN. The nearby, valid OT could be blown off downstream, mix with the warm stratosphere and mask the colder anvil below. While these scenarios are possible in mesoscale

convective systems or multicellular storms like the one shown, additional GOES imagery from the IR, visible, and water vapor channels, do not show compelling downstream plume features. The GOES-12 IR imagery, shown in Figure 5.4d, is too coarse to see many plume features necessary and visible imagery does not appear to show blown off tops downstream of the updrafts.

For all of the analysis dates, 49.4% of OTG_1 are located in regions in which the maximum $Z_H < 45$ dBZ. As shown in Figure 5.5, the majority of not co-located OTG_1 are in those regions. Figure 5.6 shows a histogram of the maximum altitude of NEXRAD 10 dBZ reflectivity (NEXRAD criteria 3) within OTG_1, relative to the ERA-I tropopause altitude. NEXRAD criteria 3 in Table 5.1 is used here, rather than NEXRAD criteria 1, in order to show the frequency and distribution of echo tops below the tropopause in OTG_1 regions. There are 234 OTG_1 ($\sim$2.4%) in regions no radar echo is observed or the maximum reflectivity measured is below 10 dBZ. Slightly over half of the OTG_1 are located in regions in which the NEXRAD radars do not observe any tropopause-overshooting echo. Because the maximum echo-top height within these OTG_1 regions are below Z_{ERA}, we know that all of those OTG_1 are all not co-located with an OTN. Approximately 56% of not co-located OTG_1 identified in regions $Z_H < 45$ dBZ contain maximum NEXRAD echo tops 2 or more km below the tropopause (not shown). This suggests the OTG_1 method is overzealously tagging events as overshoots.

5.4.4 Cloud Tops Warmer than the Tropopause

The GOES V1 algorithm weights the temperature difference between the cloud top and anvil much more heavily than the temperature difference between the cloud top and tropopause. This can cause erroneous tagging of storm tops colder than the surrounding anvil but warmer and below the tropopause as overshoots. To investigate this possibility, the difference between the cloud-top T_b and the tropopause temperature is plotted for each case. Figure 5.7a shows an example of multiple instances in which cloud tops $\Delta T_{MERRA} > 0$ are identified as OTG_1. No OTN are observed in this case. Only OTG_1 2145 has $\Delta T_{MERRA} < 0$. This storm echo is observed 1.5 km above Z_{ERA}, but it does not meet the additional criteria of 5 contiguous GridRad pixels with reflectivity $\geq$20 dBZ

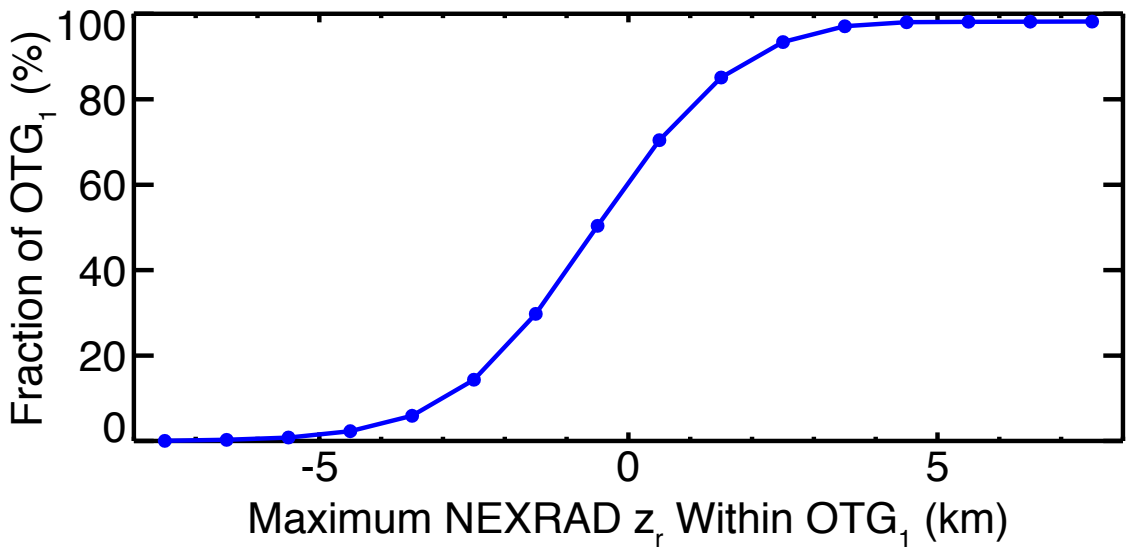

Figure 5.6: Cumulative fraction of maximum 10 dBZ ERA-I tropopause-relative echo-top height, z_r, within OTG_1. Cumulative fraction is computed by summing from left to right. The horizontal bin size is 1 km. The data points are located in the middle of each bin.

at the tropopause, so it is not flagged as an overshoot by the NEXRAD algorithm.

Nearly all of the remaining OTG_1 are in updraft regions with NEXRAD maximum z_r $<$ -2 km and are thus likely bad detections. The reason for the probable false OTG_1 identifications in this case is illustrated in Figure 5.8, which shows IR-anvil BTD for the same case. The open black circles denote OTG_1 locations, while color shaded regions without open black circles are GOES V1 overshoots with OT probability < 0.7. In the GOES V1 algorithm, larger negative IR-anvil BTD (orange and red) leads to higher OT probability. The large weight given to IR-anvil BTD causes these cloud tops to be labeled as OTs despite their actual temperatures being warmer than the tropopause temperature. This particular event is located in the southeast US where the tropopause is very cold and high ($Z_{ERA} \simeq 15.5$ km) in June. Many of the OTG_1 here are located in probable updraft regions, with $T_b < 210$ K, but the updrafts are not strong enough to penetrate the tropopause.

To quantify the impact, we removed 3663 OTG_1 that are entirely warmer than the MERRA tropopause and calculated how this impacts co-location with OTN. The number removed accounts for approximately one third of all OTG_1 identified in this study. Using NEXRAD criteria 1 in Table

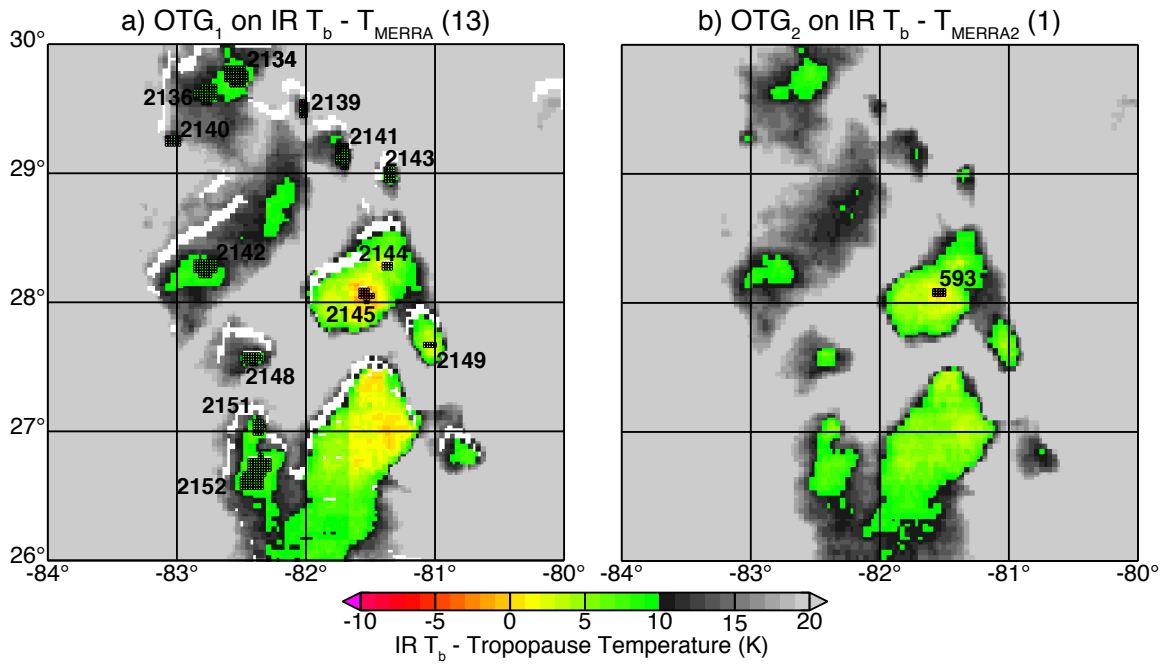

Figure 5.7: Example IR-Tropopause temperature difference map used to evaluate case study overshooting events. This example is from 14 June 2004 at 2300Z. a) IR T_b relative to the MERRA tropopause is indicated by color. The open circles indicate OTG_1 pixels. The numbers nearby the OTG_1 serve as an identification number. The number inside of the parentheses corresponds to the number of OTG_1 in the case. The white regions on the map are a result of parallax correction. b) Same as Figure 5.7a but for OTG_2 and the MERRA-2 tropopause temperature.

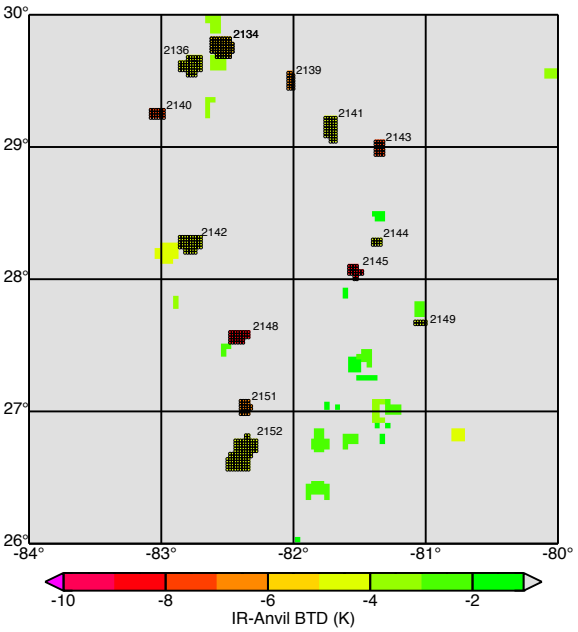

Figure 5.8: Example of an IR-anvil BTD map used to evaluate case study overshooting events. This example is from 14 June 2004 at 2300Z. Magnitude of IR T_b colder than the anvil is indicated by the shading. The open black circles indicate OTG_1 pixels. The numbers nearby each OTG_1 serve as an identification number.

5.1 as a comparison, the number of co-located OTN with OTG_1 declines ($\sim$35% co-located), while the co-located OTG_1 fraction with OTN improves to $\sim$18%. This suggests the difference between cloud top T_b and tropopause temperature (ΔT) needs to be weighted more heavily in comparison to the IR-anvil BTD, however, if it is weighted too heavily, some valid overshoot detections may be removed.

5.4.5 Valid Overshoot Cloud Top Warmer than Tropopause

As mentioned in Section 5.4.4, removing OTG_1 with cloud tops entirely warmer than the MERRA tropopause decreases the total number of OTN co-located with OTG_1. Some of this difference can be attributed to differences in ERA-I and MERRA model estimated tropopauses but tropopause differences alone do not explain every case. Figure 5.9 provides an example of a long-lived OTG_1 that is co-located with an OTN and entirely warmer than the tropopause. In this case, the OTG_1 cloud top IR T_b is approximately 208 K. The MERRA, MERRA-2, and ERA-I tropopause temperatures are nearly identical ($\sim$203.5 K). There is a strong temperature inversion

above the tropopause in this region (shown in Figure 5.9d) and the cloud top substantially overshoots the altitude of the tropopause ($\geq$ 10 dBZ echo $\sim$2.25 km above Z_{ERA} shown in Figure 5.9c).

Model-simulations have shown that in the early stages of an OT, the cloud undergoes little mixing such that, colder cloud top temperatures correspond to higher altitudes (*Setvak et al.*, 2010). In the later stages of development, the relationship between cloud top temperature and altitude are more complicated due to mass exchange with the warmer stratosphere. In addition, decaying OTs sink and warm relative to the environment. This suggests the OT in Figure 5.9 either entrains warmer stratospheric air or is sinking and warming which causes the cloud top to radiate at a warmer temperature than the tropopause. This result is observed in other cases as well. Thus, if the temperature difference between the cloud top and tropopause is weighted too heavily, the GOES OT detection scheme would likely miss these overshoots.

5.5 Comparison of NEXRAD and GOES V2

5.5.1 Improved Rejection of Cold Anvil

The GOES V2 algorithm identifies substantially fewer OTs than V1, as shown by comparing the top sections of Tables 5.1 and 5.2. Much of this is a result of reducing the number of OTs identified in stratiform regions (Figure 5.4). Similar results are found in other cases not shown here.

V2 does appear to miss some valid OTs that are detected in V1 though. For example, two V1 overshoots (89 and 96) in Figure 5.4a that are matched with OTN are not detected by the V2 algorithm (Figure 5.4b). These overshoots are located in strong updraft regions but are not identified even though the T_b is $\sim$1-3 K colder than T_{MERRA2}. In addition, the V2 method still does not identify an overshoot at longitude-latitude point 103.4°W, 37.3°N where an OTN is observed within a strong updraft. From a time series analysis, we know this overshoot is short-lived but the GOES IR imagery, provided in Figure 5.4d, shows this region is colder than its surroundings. Additional GOES visible imagery (not shown) is also indicative of an overshooting top there.

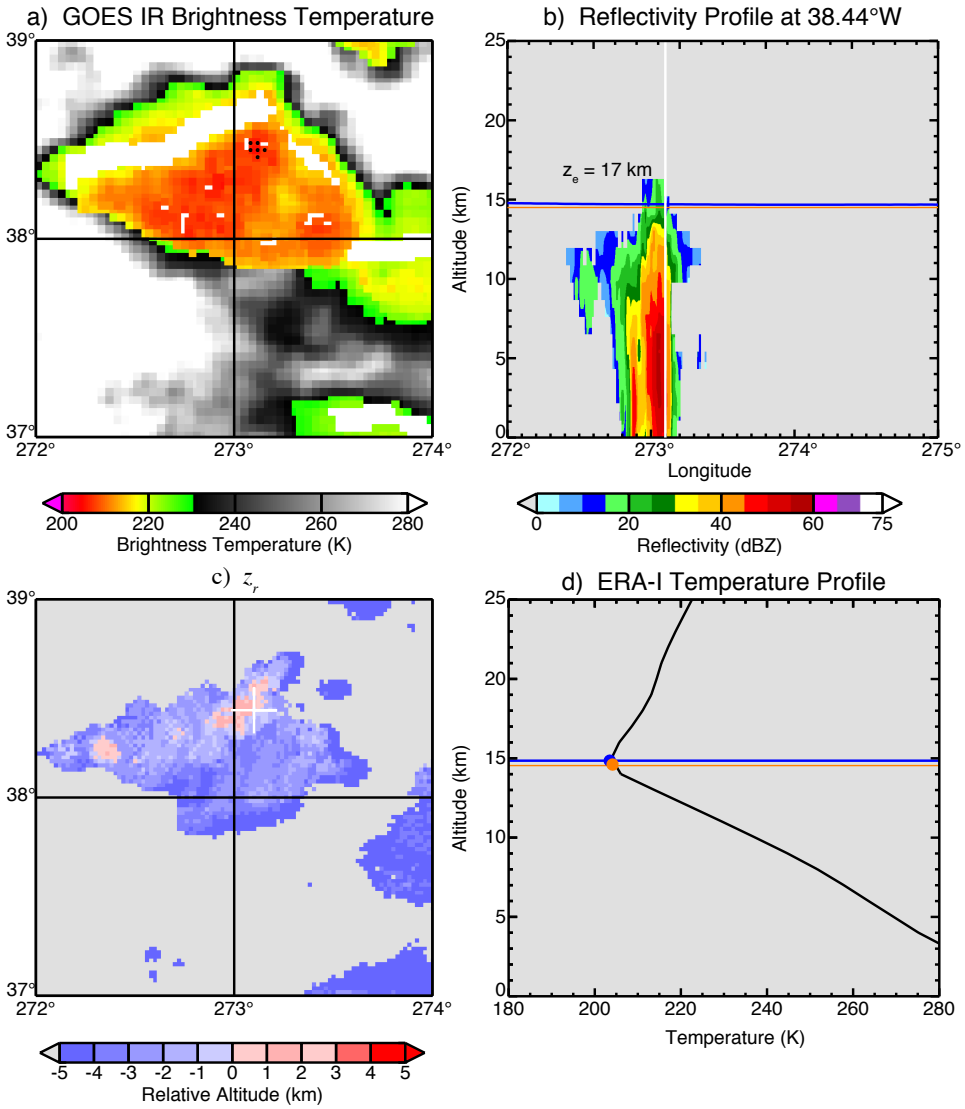

Figure 5.9: Analysis for 20 June 2006 at 2200Z. (a) Parallax corrected IR T_b map. Black circles show OTG_1 of interest location. (b) Longitude-altitude reflectivity cross-section through the middle of the OTG_1. Center of OTG_1 is marked by the vertical white line. The NEXRAD 10 dBZ echo-top altitude, z_e, is provided on the plot. The horizontal orange and blue lines indicates the ERA-I and MERRA-2 primary tropopause heights, respectively. (c) NEXRAD 10 dBZ z_r map. White crosshair marks the middle of the OTG_1. (d) ERA-I temperature profile through the middle of the OTG_1. The horizontal orange and blue lines show the primary ERA-I and MERRA-2 tropopause height, respectively. The orange and blue circles mark T_{ERA} and T_{MERRA2}, respectively.

For all of the dates analyzed, the fraction of OTG_2 detected in regions with maximum radar reflectivity $\geq$ 45 dBZ increases to 61.4%, up from 50.6% of OTG_1. Also, only 37 OTG_2 are located in regions with no echo, down from 147 OTG_1. The results in this section indicate that the V2 method reduces the false OT detection rate, but also decreases the probability of detecting a 'real' tropopause-overshooting event. As a result, the number of OTN co-located with OTG decreases from 39.9% in Version 1 to 34.2% with Version 2.

5.5.2 Improved Rejection of Cloud Tops Warmer than the Tropopause

Comparing Figures 5.7a and b shows that all of the V1 OTs with $\Delta T_{MERRA} > 0$ are not tagged by the V2 algorithm in this case. Because the V2 method weights ΔT_{MERRA2} more heavily than V1 weights ΔT_{MERRA}, OTG_2 rarely have cloud tops warmer than the tropopause. Many of the OTG_1 locations have a V2 OT probability above zero but well below the threshold of 0.7 used in this study (not shown). This suggests the Version 2 algorithm recognizes these events as overshooting the anvil but not the tropopause.

In particular, OTG_1 are frequently identified in the southeastern US even though $T_b > T_{MERRA}$. Convection is very active in the southeast US, but the tropopause is often higher, making it more difficult for updrafts to penetrate because more convective available potential energy is required (*Cooney et al.*, 2018). The improved GOES OT detection match with OTN in the southeast can be seen in Figure 5.1. This is due to the removal of many overshoot identifications with cloud top T_b warmer than the tropopause. This strongly suggests that the frequency of tropopause-overshoots in the southeast US is overestimated in *Bedka et al.* (2010).

5.5.3 Reduced Identifications of Valid Overshoots Warmer than Tropopause

Improved rejection of 'false positive' GOES overshoot identifications with cloud tops warmer than the tropopause may also reduce 'true' OT identifications that are warmer than the tropopause because the updrafts entrain warm stratospheric air. Figure 5.9 shows an example of an OTG_1 with cloud top T_b warmer than the tropopause co-located with an OTN. However, no OTG_2 is identified. The NEXRAD radars observe 10 dBZ echo $\sim$2.25 km above Z_{ERA} and the MERRA, MERRA-2,

and ERA-I tropopause temperatures are nearly identical. This suggests the larger weight given to temperature differences between the cloud top and tropopause causes GOES OT detection misses when the updraft entrains stratospheric air. This occurrence seems to be pretty rare but how often this happens is unknown and should be addressed in future OT analyses that use the GOES detection scheme.

5.5.4 Distance from Overshoots

To determine if OT position errors, which could result from instrument pointing errors or differences in observing times, are leading to missed matches between the NEXRAD and GOES OT schemes, the matching criterion is relaxed to consider matches between nearby OTs that do not directly overlap. Table 5.2 shows match frequencies for matching distances of 0 (overlap), 5, 10, and 25 km. Note that 5 km is approximately the size of one GOES-12 IR pixel. As the matching criterion is relaxed, the percentage of matches increases steadily. For a matching distance of 25 km ($\sim$0.25°), the match percentage for both NEXRAD and GOES are about 50%. For OTN that are not within 10 km of an OTG_2, the maximum z_r altitude within the OTN is $\geq$ 2 km approximately 25% of the time. This suggests the GOES Version 2 is still missing quite a few events that overshoot the tropopause by a considerable amount.

Although OTG_2 are within 10 km of the nearest OTN pixel only $\sim$37% of the time, $\sim$60% of OTG_2 are within 10 km of a 10 dBZ echo observed above the ERA-I tropopause. Therefore, the majority of OTG_2 detections are located near overshooting echo, whether or not those echoes meet the full OTN criteria.

6. SUMMARY AND CONCLUSIONS

This study compares overshooting convection identified using NEXRAD radar reflectivity data (*Cooney et al.*, 2018) with two versions of a method based on GOES IR data (*Bedka and Khlopenkov*, 2016). The comparison uses selected days with active convection in 2004 and 2006. The study area covers a large part of the contiguous United States. Overshoot detections are examined to determine potential causes of differences between the methods. The summary of the results for each hypothesis analyzed in this study are listed below.

1. Because the OTN and OTG methods calculate tropopauses from different reanalyses, we first determined if those differences had a systematic impact on OT detections. Derived MERRA and MERRA-2 tropopause temperatures are consistent with tropopause temperatures derived from ERA-I. The smoothed MERRA-2 tropopause, derived in the GOES OT V2 analysis, occasionally 'misses' the primary tropopause and instead identifies the secondary tropopause as the primary due to calculations on an irregular model vertical grid. As a result, OTN and OTG tropopause temperature differences are small but the altitude differences are large. We found this has a minimal impact on co-location frequency though because the OTG_2 method only uses tropopause temperatures and those temperatures are similar to the ERA-I tropopause temperature. In a sense, the OTG method got the right values but for the wrong reasons. We also observed instances where OT identifications were impacted by tropopause differences unrelated to missing the primary tropopause. Even without the double tropopause regions included, the smoothed MERRA-2 tropopause is often observed higher and colder than the ERA-I tropopause. As shown in *Cooney et al.* (2018), the number of overshoots that reach a given altitude relative to the tropopause falls off approximately exponentially with altitude. Therefore, using higher and colder tropopauses ultimately constrains the number of OTs observed.

2. Radar coverage over the continental US is generally good, however, the western US, offshore,

and outside US borders have poor coverage. Within the CONUS, we found radar coverage had virtually no impact on OT detection differences. In the western portion of the domain, where radar coverage is poor, very few OTG are located. Therefore, radar coverage only impacts overshoot detections outside of the CONUS and is not the predominant reason for detection differences between the NEXRAD and GOES OT detection methods within the continental US.

3. To determine if the NEXRAD overshoot criteria is too strict because it is attempting to avoid false identifications at radar echo detection limits, we show how the frequency of co-locations with OTG_1 changes after relaxing the thresholds used in *Cooney et al.* (2018). We conducted the same comparison with OTG_2 and observed similar results (not shown). There is a small difference between using 5 and 10 dBZ when identifying the echo-top height, however, the NEXRAD overshoot criteria ($Z_H \geq 20$ dBZ echo at Z_{ERA}) is found to be occasionally too strict. The overshoot criteria threshold removes a lot of noise in the radar data by ensuring the overshooting echo is part of a deep convective event and eliminating potential false positives. However, it also limits the size and number of OTN observed. Therefore, eliminating the deep convection criteria entirely is not prudent because it will result in false OTN identifications.

4. IR temperatures measured to be colder than the tropopause likely suggest the presence of an OT but this is not always true. Updrafts can rise and cool faster than the surrounding environment (*Adler and Mack*, 1986) so that cloud tops that nearly reach the altitude of the tropopause level but do not overshoot it, are colder than the tropopause temperature. While we know that this can occur, NEXRAD and GOES instrument limitations did not allow us to determine how often these events are tagged as overshoots by the GOES OT methods.

5. To determine if the GOES OT method falsely identifies events as overshoots in stratiform regions because the IR-anvil BTD is unrealistically high in situations with somewhat broken anvil cloud, we evaluated statistical trends and observed case study storm systems. Our anal-

ysis finds approximately half of OTG_1 are located outside of strong, instantaneous updraft regions. More often than not, these identifications are not co-located with an OTN. A few of these instances were a result of unrealistically high IR-anvil BTD values. GOES Version 2 recognized this issue in V1 and removes many of the V1 identifications in stratiform regions, particularly those far away from updraft regions.

6. For not co-located OTG_1 near updrafts, there are a few instances of potential blown off tops or above-anvil cirrus observed in the case study storms. Identifying above-anvil cirrus was difficult to assess, however, because GOES-12 IR imagery is too coarse to see a lot of plume features in multicellular storms and visible imagery requires the sun, so it is not always available. Newer GOES satellites (GOES-16 and GOES-17) make observations at higher spatial and temporal resolution where these features can be better observed than GOES-12. Future work should compare GOES overshoot identifications from the newer satellites with NEXRAD to gain more insight on these identifications.

7. Nearly a third of OTG_1 are entirely warmer than the MERRA tropopause, most of which are detected in the southeast US. The southeast US has very strong convective events, but the tropopause is often higher there than in the central plains US, making it more difficult to overshoot. Because the OTG_2 method gives more weight to cloud top T_b and tropopause temperature differences than the OTG_1 method, OTG_2 tops are rarely warmer than the tropopause. This removes many false positive identifications in the southeast US from the V1 method.

8. IR temperatures measured to be colder than the tropopause likely suggest the presence of an OT. Long-lived OTs though can entrain a substantial amount of warm stratospheric air, causing the cloud top to radiate at a warmer temperature than the tropopause and ultimately lead to the GOES detection scheme missing valid tropopause-overshoots. We identified examples of this during the case study analysis but, due to the complex relationship between altitude and temperature, cannot quantify the detection impact. Because GOES V2 is weighted more heavily towards temperature differences between the cloud top and tropopause than V1, V2

more frequently misses these valid OTs.

Using temperature differences as a proxy for identifying tropopause-overshooting convection is a very difficult task. GOES V1 appears to make a large number of false positive detections. These are primarily due to failing to reject OT candidates with brightness temperatures warmer than the tropopause and putting too much weight on the temperature difference between the cloud top and its surrounding anvil. Version 1 to Version 2 shows marked improvement in the identifications, however, the more strict Version 2 criteria eliminates some valid Version 1 overshoot detections in updraft regions. It is also rare for a NEXRAD overshoot to be co-located with a V2 OT if it is not also co-located with a V1 OT. These instances primarily occur when the MERRA and MERRA-2 tropopause temperatures are vastly different ($T_{MERRA2} > T_{MERRA}$) or the different parallax corrections result in an OTG_2 overlapping an OTN rather than being directly adjacent. Therefore, Version 2 significantly lowers the false-alarm rate but also slightly lowers the probability of capturing a tropopause-overshooting event.

Even though the GOES and NEXRAD methods do not observe perfectly aligned overshoots, the OTs are typically detected within the same storm system. Over half of the OTN are ≤ 25 km from the nearest OTG_2 and nearly half of the OTG_2 are ≤ 25 km from an OTN. These fractions are far larger than the exact overlap counts and better represent how well the GOES and NEXRAD OT detection methods match because it shows the methods are observing overshoots within the same storm regions. However, even with the relaxed matching, it is still far from perfect and improvements in the algorithms can be made.

One way to make the NEXRAD method less strict but still retain the deep convection criteria is to require only one or two of the contiguous overshooting pixels contain at least a 20 dBZ echo at Z_{ERA}, rather than all of them. In theory, this would still ensure the overshoot is from deep convection but without being too restrictive. This could also be useful for calculating the volume of overshooting echo in order to estimate the amount of mass exchange across the tropopause. Testing would need to be done, however, to ensure erroneous OTs are not frequently identified by relaxing the NEXRAD criteria in this way.

Future GOES algorithms could be improved by using additional GOES imagery channels in conjunction with the IR channel. On their own, additional satellite imagery channels has drawbacks to detecting OTs but together, they could provide a more reliable detection system. Previous analyses have used the water vapor channel T_b minus the IR T_b because the presence of stratospheric water vapor injection by OTs has been theorized to correlate to positive values. Some studies have shown this to be true (*Young et al.*, 2012) while others have found that it cannot always differentiate between OTs and anvil (*Bedka et al.*, 2010). The GOES visible channel can also be used to detect OTs. Visible imagery is not always available but when it is, overshoots exhibit characteristic texture and shadowing upon the surrounding anvil (*Bedka and Khlopenkov*, 2016). Determining how each GOES imagery channel can be weighted to detect OTs will be extremely difficult though. Some of this information could be interpreted physically, yet in practice it is difficult to know which channels are most important or "true" (*Berendes et al.*, 2008).

REFERENCES

(2019), American Meteorological Society Glossary of Meteorology.

Adler, R. F., and R. A. Mack (1986), Thunderstorm cloud top dynamics as inferred from satellite observations and a cloud top parcel model, *J. Atmos. Sci.*, *43*, 1945–1960.

Adler, R. F., D. D. Fenn, and D. A. Moore (1981), Spiral feature observed at top of rotating thunderstorm, *Mon. Wea. Rev.*, *109*, 1124–1129.

Adler, R. F., M. J. Markus, and D. D. Fen (1983), Thunderstorm top structure observed by aircraft overflights with an infrared radiometer, *J. Climate Appl. Meteor.*, *22*, 579–593.

Anderson, J. G., D. M. Wilmouth, J. B. Smith, and D. S. Sayres (2012), UV dosage levels in summer: Increased risk of ozone loss from convectively injected water vapor, *Science*, *337*, 835–839, doi:10.1126/science.1222978.

Anderson, J. G., D. K. Weisenstein, K. P. Bowman, C. R. Homeyer, J. B. Smith, D. M. Wilmouth, D. S. Sayres, J. E. Klobas, S. S. Leroy, J. A. Dykema, and S. C. Wofsy (2017), Stratospheric ozone over the United States in summer linked to observations of convection and temperature via chlorine and bromine catalysis, *Proc. Nat. Acad. Sci.*, *114*, E4905–E4913, doi:10.1073/pnas.1619318114.

Bedka, K., J. Brunner, R. Dworak, W. Feltz, J. Otkin, and T. Greenwald (2010), Objective satellite-based detection of overshooting tops using infrared window channel brightness temperature gradients, *J. Appl. Meteor. Clim.*, *49*, 181–202, doi:10.1175/2009JAMC2286.1.

Bedka, K. M., and K. Khlopenkov (2016), A probabilistic multispectral pattern recognition method for detection of overshooting cloud tops using passive satellite imager observations, *J. App. Met. Clim.*, *55*(9), 1983–2005.

Berendes, T. A., J. R. Mecikalski, W. M. M. Jr., K. M. Bedka, and U. S. Nair (2008), Convective cloud identification and classification in daytime satellite imagery using standard deviation limited adaptive clustering, *J. Geophys. Res.*, *113*(D20), 207, doi:10.1029/2008JD010287.

Bosilovich, M., and R. Lucchesi (2016), Merra-2:file specification, *Office Note 9*, Global Modeling and Assimilation Office.

Cooney, J. W., K. P. Bowman, C. R. Homeyer, and T. M. Fenske (2018), Ten-year analysis of tropopause-overshooting convection using gridrad data, *J. Geophys. Res. Atmos.*, *123*, 329–343.

Dee, D. P., S. M. Uppala, A. J. Simmons, P. Berrisford, P. Poli, S. Kobayashi, U. Andrae, M. A. Balmaseda, G. Balsamo, P. Bauer, P. Bechtold, A. C. M. Beljaars, L. van de Berg, J. Bidlot, N. Bormann, C. Delsol, R. Dragani, M. Fuentes, A. J. Geer, L. Haimberger, S. B. Healy, H. Hersbach, E. V. Hólm, L. Isaksen, P. Kållberg, M. Köhler, M. Matricardi, A. P. McNally, B. M. Monge-Sanz, J.-J. Morcrette, B.-K. Park, C. Peubey, P. de Rosnay, C. Tavolato, J.-N. Thépaut, and F. Vitart (2011), The era-interim reanalysis: configuration and performance of the data assimilation system, *Q. J. R. Meteorol. Soc.*, *137*(656), 553–597, doi:10.1002/qj.828.

Dessler, A. E., and S. C. Sherwood (2004), Effect of convection on the summertime extratropical lower stratosphere, *J. Geophys. Res.*, *109*(D23), 301, doi:10.1029/2004JD005209.

FAA (2019), Fact sheet – turbulence.

Forster, P. M. D., and K. P. Shine (1999a), Stratospheric water vapor changes as a possible contributor to observed stratospheric cooling, *Geophysical Research Letters*, *26*(21), 3309–3312.

Forster, P. M. D., and K. P. Shine (1999b), Stratospheric water vapor changes as a possible contributor to observed stratospheric cooling, *Geophysical Research Letters*, *26*(21), 3309–3312.

Fujita, T. T. (1981), Mesoscale aspects of convective storms, *Nowcasting: Mesoscale Observations and Short-Range Prediction., Proceedings of an International Symposium*.

Fujita, T. T. (1982), Principle of stereoscopic height computations and their applications to stratospheric cirrus over severe thunderstorms, *J. Met. Soc. Japan*, *60*(1), 355–368.

Griffin, S. M., K. M. Bedka, and C. S. Velden (2016), A method for calculating the height of overshooting convective cloud tops using satellite-based ir imager and cloudsat profiling radar observations, *J. Appl. Meteor. Climatol.*, pp. 479–491.

Herman, R., E. Ray, K. Rosenlof, K. Bedka, M. Schwartz, W. Read, R. Troy, K. Chin, L. Christensen, D. Fu, R. Stachnik, T. Bui, and J. Dean-Day (2017), Enhanced stratospheric water vapor over the summertime continental united states and the role of overshooting convection, *Atmospheric Chemistry and Physics*, *17*(9), 6113–6124.

Heymsfield, G. M., R. Fulton, and J. D. Spinhirne (1991), Aircraft overflight measurements of midwest severe storms: Implications an geosynchronous satellite interpretations, *Monthly Weather Review*, *119*, 436–456.

Hillger, D. W., T. J. Schmit, and J. M. Daniels (2003), Imager and sounder radiance and product validations for the goes-12 science test, *Tech. rep.*, NOAA.

Holton, J. R., P. H. Haynes, M. E. McIntyre, A. R. Douglass, R. B. Rood, and L. Pfister (1995), Stratosphere-troposphere exchange, *Rev. Geophys.*, *33*, 403–439, doi:10.1029/95RG02097.

Homeyer, C. R. (2014), Formation of the Enhanced-V infrared cloud top feature from high-resolution three-dimensional radar observations, *J. Atmos. Sci.*, *71*, 332–348, doi:10.1175/JAS-D-13-079.1.

Homeyer, C. R., and K. P. Bowman (2017), Algorithm Description Document for Version 3.1 of the Three-Dimensional Gridded NEXRAD WSR-88D Radar (GridRad) Dataset, *Tech. rep.*, GridRad.org, doi:http://gridrad.org/pdf/GridRad-v3.1-Algorithm-Description.pdf.

Homeyer, C. R., and M. R. Kumjian (2015), Microphysical characteristics of overshooting

convection from polarimetric radar observations, *J. Atmos. Sci.*, *72*, 870–891, doi:10.1175/JAS-D-13-0388.1.

Homeyer, C. R., L. L. Pan, S. W. Dorsi, L. M. Avallone, A. J. Weinheimer, A. S. O'Brien, J. P. DiGangi, M. A. Zondlo, T. B. Ryerson, G. S. Diskin, and T. L. Campos (2014), Convective transport of water vapor into the lower stratosphere observed during double-tropopause events, *J. Geophys. Res.*, *119*, 10,941–10,958, doi:10.1002/2014JD021485.

Lane, T. P., R. D. Sharman, T. L. Clark, and H.-M. Hsu (2003), An investigation of turbulence generation mechanisms above deep convection, *Journal of Atmospheric Science*, *60*, 1297–1321.

Levizzani, V., and M. Setvak (1996), Multispectral, high-resolution satellite observations of plumes on top of convective storms, *Journal of Atmospheric Science*, *53*(3), 361–369.

Negri, A. J. (1982), Cloud-top structure of tornado storms on 10 april 1979 from rapid scan and stereo satellite observations, *Bull. Amer. Meteor. Soc.*, *63*, 1851–1859.

Pan, L. L., C. R. Homeyer, S. Honomichl, B. A. Ridley, M. Weisman, M. C. Barth, J. W. Hair, M. A. Fenn, C. Butler, G. S. Diskin, J. H. Crawford, T. B. Ryerson, I. Pollack, J. Peischl, and H. Huntrieser (2014), Thunderstorms enhance tropospheric ozone by wrapping and shedding stratospheric air, *Geophys. Res. Lett.*, *in press*, doi:10.1002/2014GL061921.

Peng, G. (2014), Analysis, reanalysis, forecast—what's the difference?, online.

Rienecker, M. M., M. J. Suarez, R. Gelaro, R. Todling, J. Bacmeister, E. Liu, M. G. Bosilovich, S. D. Schubert, L. Takacs, G.-K. Kim, S. Bloom, J. Chen, D. Collins, A. Conaty, A. da Silva, W. Gu, J. Joiner, R. D. Koster, R. Lucchesi, A. Molod, T. Owens, S. Pawson, P. Pegion, C. R. Redder, R. Reichle, F. R. Robertson, A. G. Ruddick, M. Sienkiewicz, and J. Woollen (2011), Merra: Nasa's modern-era retrospective analysis for research and applications, *J. Climate Appl. Meteor.*, *24*, 3624–3648.

Setvak, M., D. T. Lindsey, P. Novak, P. K. Wang, M. Radova, J. Kerkmann, L. Grasso, S.-H. Su, R. M. Rabin, J. Stastka, and Z. Charvat (2010), Satellite-observed cold-ring-shaped features atop deep convective clouds, *Atmos. Res.*, *97*, 80–96.

Smith, J. B., D. M. Wilmouth, K. Bedka, K. P. Bowman, C. R. Homeyer, J. A. Dykema, M. R. Sargent, C. E. Clapp, S. S. Leroy, D. S. Sayres, J. M. Dean-Day, T. P. Bui, and J. G. Anderson (2017), A case study of convectively sourced water vapor observed in the overworld stratosphere over the united states, *Journal of Geophysical Research: Atmospheres*, *122*(17), 9529–9554.

Solomon, D. L., K. P. Bowman, and C. R. Homeyer (2016), Tropopause-penetrating convection from three-dimensional gridded NEXRAD data, *J. App. Met. Clim.*, *55*, 465–478, doi:10.1175/JAMC-D-15-0190.1.

Stohl, A., H. Wernli, P. James, M. Bourqui, C. Forster, M. A. Liniger, P. Seibert, and M. Sprenger (2003), A new perspective of stratosphere-troposphere exchange, *Bull. Amer. Meteor. Soc.*, *84*, 1565–1573, doi:10.1175/BAMS-84-11-1565.

WMO (1957), Meteorology - a three-dimensional science: Second session of the commission for aerology, *WMO Bulletin*, *VI*(4), 134–138.

Young, A. H., J. J. Bates, and J. A. Curry (2012), Complementary use of passive and active remote sensing for detection of penetrating convection from cloudsat, calipso, and aqua modis, *Journal of Geophysical Research*, *117*.